

# Gravitational Waves from First-Order Phase Transition in a Simple Axion-Like Particle Model

---

P. S. Bhupal Dev,<sup>a</sup> Francesc Ferrer,<sup>a</sup> Yiyang Zhang,<sup>a</sup> Yongchao Zhang<sup>a,b</sup>

<sup>a</sup>*Department of Physics and McDonnell Center for the Space Sciences, Washington University, St. Louis, MO 63130, USA*

<sup>b</sup>*Center for High Energy Physics, Peking University, Beijing 100871, China*

**ABSTRACT:** We consider a gauge-singlet complex scalar field  $\Phi$  with a global  $U(1)$  symmetry that is spontaneously broken at some high energy scale  $f_a$ . As a result, the angular part of the  $\Phi$ -field becomes an axion-like particle (ALP). We show that if the  $\Phi$ -field has a non-zero coupling  $\kappa$  to the Standard Model Higgs boson, there exists a large region in the  $(f_a, \kappa)$  parameter space where the global  $U(1)$  symmetry-breaking induces a strongly first order phase transition, thereby producing stochastic gravitational waves that are potentially observable in current and future gravitational-wave detectors. In particular, we find that future gravitational-wave experiments such as LISA, BBO and aLIGO+ could probe a broad range of the energy scale  $10^3 \text{ GeV} \lesssim f_a \lesssim 10^8 \text{ GeV}$ , independent of the ALP mass. Since all the ALP couplings to the Standard Model particles are proportional to inverse powers of the energy scale  $f_a$  (up to model-dependent  $\mathcal{O}(1)$  coefficients), the gravitational-wave detection prospects are largely complementary to the current laboratory, astrophysical and cosmological probes of the ALP scenarios.

---

## Contents

<b>1</b>	<b>Introduction</b>	<b>1</b>
<b>2</b>	<b>Scalar Potential in the ALP model</b>	<b>3</b>
2.1	Tree-level potential	3
2.2	Effective finite-temperature potential	4
<b>3</b>	<b>Gravitational wave spectrum</b>	<b>4</b>
3.1	First-order phase transition	4
3.2	Bounce solution	6
3.3	Production mechanism for gravitational waves	6
3.4	Critical temperature	9
3.5	Bubble nucleation	9
3.6	Detection prospects	10
<b>4</b>	<b>Comparison with other ALP constraints</b>	<b>13</b>
4.1	Low-energy effective couplings of ALP	13
4.2	Coupling to photon	14
4.3	Coupling to electron	17
4.4	Coupling to nucleon	18
<b>5</b>	<b>Prospects from precision Higgs data at future colliders</b>	<b>19</b>
<b>6</b>	<b>Conclusion</b>	<b>21</b>
<b>A</b>	<b>Power-law Integrated Sensitivity Curves</b>	<b>21</b>

---

## 1 Introduction

Axion-like particles (ALPs) are light gauge-singlet pseudoscalar bosons that couple weakly to the Standard Model (SM) and generically appear as the pseudo-Nambu-Goldstone boson (pNGB) in theories with a spontaneously broken global  $U(1)$  symmetry. ALPs could solve some of the open questions of the SM, such as the strong CP problem via the Peccei-Quinn mechanism [1] and the hierarchy problem via the relaxion mechanism [2]. They could also play an important role in cosmology such as inflation [3–5], dark matter [6–8], dark energy [9–12], and baryogenesis [13, 14]. There are recent proposals involving axions to simultaneously address several open issues of the SM in one stroke [15–17].

A common characteristic among ALPs is that their coupling to SM particles is suppressed by inverse powers of the  $U(1)$  symmetry breaking energy scale,  $f_a$ . This energy scale can be identified as the vacuum expectation value (VEV) of a SM-singlet complex

scalar field  $\Phi$ , i.e.  $\langle \Phi \rangle = f_a/\sqrt{2}$  which is assumed to be much larger than the electroweak scale  $v_{\text{ew}} \simeq 246.2$  GeV to evade current experimental limits [18, 19]. The ALP field  $a$  then arises as the massless excitation of the angular part of the  $\Phi$ -field:

$$\Phi(x) = \frac{1}{\sqrt{2}} [f_a + \phi(x)] e^{ia(x)/f_a}. \quad (1.1)$$

The particle excitation of the modulus  $\phi$  of the  $\Phi$ -field gets a large mass  $m_\phi \sim f_a$ , while the angular part  $a$  becomes a pNGB that acquires a much smaller mass  $m_a$  from explicit low energy  $U(1)$ -breaking effects. Thus, for the low-energy phenomenology of ALPs, the modulus part  $\phi$  can be safely integrated out, and the only experimentally relevant parameters are  $m_a$  and  $f_a$ .

In this paper, we show that the dynamics of the modulus  $\phi$ -field around the  $f_a$  scale can provide complementary constraints on the ALP scenario. In particular, if the parent  $\Phi$ -field has a non-zero coupling to the SM Higgs doublet  $H$ , the  $U(1)$  symmetry breaking at the  $f_a$ -scale could induce a strongly first-order phase transition (FOPT), giving rise to stochastic gravitational wave (GW) signals that are potentially observable in current and future GW detectors. We find that GW signals of strength up to  $h^2\Omega_{\text{GW}} \sim 10^{-8}$  (where  $\Omega_{\text{GW}}$  is the fraction of the total energy density of the universe in the form of GWs today and  $h = 0.674 \pm 0.005$  is the current value of the Hubble parameter in units of  $100 \text{ km s}^{-1} \text{ Mpc}^{-1}$  [20]) could be generated. Future GW observatories like aLIGO+ [21], TianQin [22], Taiji [23], LISA [24, 25], ALIA [26], MAGIS [27], DECIGO [28], BBO [30], Cosmic Explorer (CE) [31] and Einstein Telescope (ET) [32] can probe a broad range  $10^3 \text{ GeV} \lesssim f_a \lesssim 10^8 \text{ GeV}$ , *independent* of the ALP mass.

At low energies, the heavy modulus  $\phi$  decouples, and we are left with the ALP  $a$ , which has only derivative couplings to the SM particles. These are generated via effective higher-dimensional operators [33], and are proportional to inverse powers of  $f_a$ , up to model-dependent  $\mathcal{O}(1)$  coefficients. The effective ALP couplings to photons, electrons and nucleons are strongly constrained by a number of laboratory, astrophysical and cosmological observables [19]. However, current and future low-energy constraints depend on the ALP mass  $m_a$ , while we find that the GW prospects in the  $(m_a, f_a)$  plane are largely complementary. For instance, if a stochastic GW signal was found with the frequency dependence predicted by the FOPT<sup>1</sup>, this would point to a limited range of  $f_a$  in a given ALP model, which might lead to a *positive* signal in some of the future laboratory and/or astrophysical searches of ALPs. On the other hand, if we fix the ALP mass  $m_a$ , then current ALP constraints exclude certain ranges of  $f_a$ . If a GW signal is found in the frequency range corresponding to the excluded range of  $f_a$ , then the underlying simple ALP model has to be extended to account for the GW signal.

The rest of the paper is organized as follows: in section 2 we provide the details of the ALP model, and we compute the one-loop effective scalar potential at both zero and finite temperature. In section 3 we calculate the GW emission from a strong FOPT

---

<sup>1</sup>If the GW signal was indeed from the FOPT in the ALP model. The frequency dependence in this scenario is generically different and can be distinguished from other GW sources, like inflation [34–39] or unresolved binary black hole mergers [40].

at the scale  $f_a$ , including bubble collision, sound wave (SW) and magnetohydrodynamic (MHD) turbulence contributions. The complementary reach of laboratory, astrophysical and cosmological observations is presented in Section 4, and the constraints from future precision Higgs data on the ALP model are discussed in section 5. We summarize and conclude in section 6. The method used to obtain the power-law integrated sensitivity curves for future GW experiments is described in appendix A.

## 2 Scalar Potential in the ALP model

### 2.1 Tree-level potential

The coupling between the SM Higgs doublet  $H$  and the complex field  $\Phi$  is described by the tree-level potential

$$\mathcal{V}_0 = -\mu^2|H|^2 + \lambda|H|^4 + \kappa|\Phi|^2|H|^2 + \lambda_a \left( |\Phi|^2 - \frac{1}{2}f_a^2 \right)^2. \quad (2.1)$$

The SM Higgs doublet can be parameterized as  $H = (G_+, (h + iG_0)/\sqrt{2})$ , with  $h$  the SM Higgs and  $G_0, G_+$  the Goldstone bosons that become the longitudinal components of the SM  $Z$  and  $W$  bosons. The complex field  $\Phi$  can be expressed in the form given by Eq. (1.1). At an energy scale around  $f_a$ , a phase transition (PT) occurs and the global  $U(1)$  symmetry is broken. The field  $\phi$  gets a VEV  $\langle\phi\rangle = f_a/\sqrt{2}$ , and the associated pNGB  $a$  is identified as the physical ALP. Depending on the parameters  $f_a, \kappa$  and  $\lambda_a$ , the PT may be strongly first order, in which case it would generate a spectrum of GWs that could be detected in current or future GW experiments [41], as detailed in Section 3. We note that at this stage the ALP  $a$  is not involved in the scalar potential, Eq. (2.1), nor in the GW emission from the high-energy scale PT. The low-energy effective couplings of  $a$  to SM particles will be discussed in Section 4.1.

In terms of the real scalar field components, the tree-level potential in Eq. (2.1) can be re-written as:

$$\begin{aligned} \mathcal{V}_0 = & \frac{\lambda_a}{4} (\phi^2 - f_a^2)^2 + \left[ \frac{\kappa}{2}\phi^2 - \mu^2 \right] \left( \frac{1}{2}h^2 + \frac{1}{2}G_0^2 + G_+G_- \right) \\ & + \lambda \left[ \frac{1}{2}h^2 + \frac{1}{2}G_0^2 + G_+G_- \right]^2. \end{aligned} \quad (2.2)$$

Here  $f_a, \kappa$  and  $\lambda_a$  are taken as free parameters, while the  $\mu$  parameter can be obtained from the quartic couplings and the SM Higgs mass. The scalar field  $\phi$  is the dynamical field during the PT, and it obtains a non-zero VEV  $\langle\phi\rangle$  after the PT.

At the electroweak scale, the effective potential for the SM Higgs is:

$$\mathcal{V}_0^{(\text{EW})}(h) = - \left[ \frac{1}{2}\mu^2 - \frac{1}{4}\kappa\langle\phi\rangle^2 \right] h^2 + \frac{\lambda}{4}h^4 = -\frac{1}{2}\mu_{\text{eff}}^2 h^2 + \frac{\lambda}{4}h^4. \quad (2.3)$$

Since  $\mu_{\text{eff}} \sim 100$  GeV and  $\langle\phi\rangle \sim f_a$ , to obtain the observed Higgs mass,  $m_h = 125$  GeV, we will take  $\mu^2 \simeq \kappa f_a^2/2$  as long as  $f_a \gg m_h$ .

## 2.2 Effective finite-temperature potential

At finite temperature  $T \neq 0$ , the effective one-loop potential of the scalar fields is [42–45]:

$$\mathcal{V}(\phi, T) = \mathcal{V}_0(\phi) + \mathcal{V}_{\text{CW}}(\phi) + \mathcal{V}_T(\phi, T), \quad (2.4)$$

where  $V_{\text{CW}}$  is the Coleman-Weinberg potential [46] that contains all the one-loop corrections at zero temperature with vanishing external momenta, and  $V_T$  describes the finite-temperature corrections. Working in the Landau gauge to avoid ghost-compensating terms, the Coleman-Weinberg potential reads:

$$\mathcal{V}_{\text{CW}}(\phi) = \sum_i (-1)^F n_i \frac{m_i^4(\phi)}{64\pi^2} \left[ \log \frac{m_i^2(\phi)}{\Lambda^2} - C_i \right]. \quad (2.5)$$

The sum runs over all the particles that couple to the  $\phi$  field (notice that massless particles do not contribute). In Eq. (2.5),  $F = 1$  for fermions and 0 for bosons;  $n_i$  is the number of degrees of freedom of each particle;  $C_i = 3/2$  for scalars and fermions and  $5/6$  for gauge bosons; and  $\Lambda$  is the renormalization scale, which will be set to  $f_a$  throughout this paper.

The finite-temperature corrections are given by:

$$\mathcal{V}_T(\phi, T) = \sum_i (-1)^F n_i \frac{T^4}{2\pi^2} J_{B/F} \left( \frac{m_i^2(\phi)}{T^2} \right), \quad (2.6)$$

where the thermal functions are:

$$J_{B/F}(y^2) = \int_0^\infty dx x^2 \log \left[ 1 \mp \exp \left( -\sqrt{x^2 + y^2} \right) \right]. \quad (2.7)$$

Here, the minus sign “−” is for bosons and the positive sign “+” for fermions. We also need to include the resummed daisy corrections, that add a temperature-dependent term  $\Pi_i(T)$  to the field-dependent mass  $m_i^2$  [45]. To leading order, we have in the ALP model:

$$\Pi_h(T) = \Pi_{G_{0,\pm}}(T) = \frac{1}{48} (9g_2^2 + 3g_1^2 + 12y_t^2 + 24\lambda + 4\kappa) T^2, \quad (2.8)$$

$$\Pi_\phi(T) = \frac{1}{3} (\kappa + 2\lambda_a) T^2. \quad (2.9)$$

Effectively, the mass terms  $m_i^2$  in Eqs. (2.5) and (2.6) get replaced by  $m_i^2 + \Pi_i(T)$ .

The effective potential in Eq. (2.4) could become complex due to  $m_i^2$  being negative. This is related to particle decay and does not affect the computation of the dynamics of PT (see e.g. [47–49] for more details). In the numerical calculations in Section 3 we will always take the real part of the effective potential.

## 3 Gravitational wave spectrum

### 3.1 First-order phase transition

Fixing the decay constant  $f_a$  at a specific value, we scan the region in  $(\kappa, \lambda_a)$  parameter space where a FOPT can take place. In particular, we evaluate the effective potential

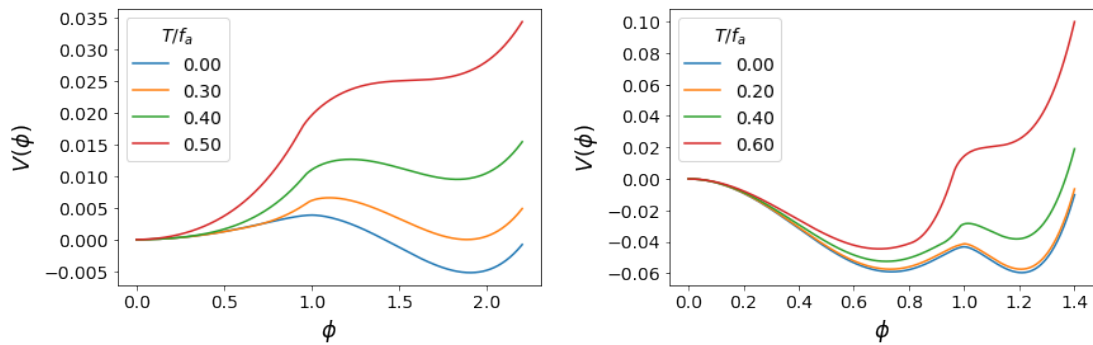


**Figure 1.** Two different cases of FOPT in the ALP model: the type-A (local minimum at  $\phi = 0$ ) in the left panel and type-B (local minimum at  $\phi \neq 0$ ) in the right panel.

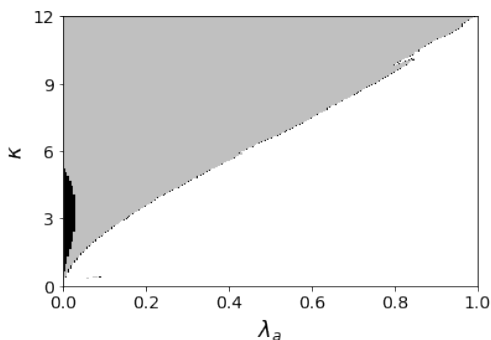


**Figure 2.** The parameter space for a FOPT in the ALP model with  $f_a = 10^7$  GeV. The type-A case is depicted in black and type-B in gray.

for given values of  $(\kappa, \lambda_a)$  to look for regions where there is a valid critical temperature  $T_c$ . Here,  $T_c$  is defined as the temperature at which the two local minima of the effective potential are degenerate. We use the package `CosmoTransitions` [50] for the numerical work and the results are given in the following subsections.

It turns out that, in the simple ALP model, there are two different types of FOPT, depending on whether the local minimum of the potential is at  $\phi = 0$  or  $\phi \neq 0$ . We refer to the two cases as type-A and type-B respectively, and sample effective potentials are shown in Fig. 1. Notice that the potential barrier between the meta-stable phase and the true vacuum does not vanish at  $T = 0$ , indicating a strong FOPT. The parameter space for the two FOPT cases of type-A and type-B is depicted in Fig. 2 in black and gray respectively, with the benchmark value  $f_a = 10^7$  GeV. In addition, we have found that the interesting range of the two parameters falls within  $\kappa \in (0, 12]$  and  $\lambda_a \in (0, 1.0]$ , beyond which the quartic coupling  $\kappa$  becomes non-perturbative. We have also checked the parameter space for other values of  $f_a$  and found that the viable regions of  $(\kappa, \lambda_a)$  do not change significantly.

### 3.2 Bounce solution

The decay rate of the false vacuum is [51–53]:

$$\Gamma(T) \simeq \max \left[ T^4 \left( \frac{S_3}{2\pi T} \right)^{3/2} \exp(-S_3/T), \left( \frac{S_4}{2\pi R_0^2} \right)^2 \exp(-S_4) \right], \quad (3.1)$$

where the first term corresponds to thermally induced decays and the second term is the quantum-tunneling rate. In Eq. (3.1)  $S_3$  and  $S_4$  are respectively the three- and four-dimensional Euclidean actions for the  $O(3)$  and  $O(4)$  symmetric tunnelling (“bounce”) solutions, and  $R_0$  is the size of the bubble. For quantum tunneling,

$$S_4 = \int d^4x \left[ \frac{1}{2} \left( \frac{d\phi}{dt} \right)^2 + \frac{1}{2} (\nabla\phi)^2 + \mathcal{V}(\phi, T) \right], \quad (3.2)$$

where  $\phi(r)$  is the solution of the  $O(4)$ -symmetric instanton (with  $r = \sqrt{\mathbf{r}^2 + t^2}$ ):

$$\frac{d^2\phi}{dr^2} + \frac{3}{r} \frac{d\phi}{dr} = \mathcal{V}'(\phi, T). \quad (3.3)$$

For thermally-induced decay,

$$S_3 = \int d^3x \left[ (\nabla\phi)^2 + \mathcal{V}(\phi, T) \right], \quad (3.4)$$

where  $\phi(r)$  is the  $O(3)$ -symmetric solution of

$$\frac{d^2\phi}{dr^2} + \frac{2}{r} \frac{d\phi}{dr} = \mathcal{V}'(\phi, T). \quad (3.5)$$

### 3.3 Production mechanism for gravitational waves

The GW signal from a FOPT consists of three main components: the scalar field contribution during collision of bubble walls [54–59], the sound wave in the plasma after bubble collisions [60–63], and the MHD turbulence in the plasma after bubble collisions [64–68]. Assuming the three components can approximately be linearly superposed, the total strength of GWs produced reads:

$$h^2\Omega_{\text{GW}} \simeq h^2\Omega_\phi + h^2\Omega_{\text{SW}} + h^2\Omega_{\text{MHD}}. \quad (3.6)$$

Note that the global  $U(1)$  symmetry breaking could also generate cosmic strings, which then annihilate to produce GWs [69]. However, this effect turns out to be subdominant for the energy scales under consideration here.

The envelope approximation is often used in calculating the GWs from the scalar  $\phi$  contribution, and numerical simulations reveal that [56, 70]:

$$h^2\Omega_\phi(f) \simeq 1.67 \times 10^{-5} \left( \frac{H_*}{\beta} \right)^2 \left( \frac{\kappa_\phi \alpha}{1 + \alpha} \right)^2 \left( \frac{100}{g_*} \right)^{1/3} \left( \frac{0.11 v_w^3}{0.42 + v_w^2} \right) S_{\text{env}}(f),$$

where  $f$  is the frequency;  $g_*$  is the number of relativistic degrees of freedom in the plasma at the temperature  $T_*$  when the GWs are generated;  $H_*$  is the Hubble parameter at  $T_*$ ;

$v_w$  is the bubble wall velocity in the rest frame of the fluid;  $\alpha = \rho_{\text{vac}}/\rho_{\text{rad}}^*$  is the ratio of the vacuum energy density  $\rho_{\text{vac}}$  released in the PT to that of the radiation bath  $\rho_{\text{rad}}^* = g_*\pi^2 T_*^4/30$ ;  $\beta/H_*$  measures the rate of the PT;  $\kappa_\phi$  measures the fraction of vacuum energy that is converted to gradient energy of the  $\phi$  field; and  $S_{\text{env}}(f)$  parameterizes the spectral shape of the GW radiation,

$$S_{\text{env}}(f) = \frac{3.8 (f/f_{\text{env}})^{2.8}}{1 + 2.8 (f/f_{\text{env}})^{3.8}}. \quad (3.7)$$

The peak frequency  $f_{\text{env}}$  of the  $\phi$  contribution to the spectrum is determined by  $\beta$  and by the peak frequency  $f_* = 0.62\beta/(1.8 - 0.1v_w + v_w^2)$  [56] at the time of GW production,

$$f_{\text{env}} = \left(\frac{f_*}{\beta}\right) \left(\frac{\beta}{H_*}\right) h_*. \quad (3.8)$$

Assuming the Universe is radiation-dominated after the PT and has expanded adiabatically ever since, the inverse Hubble time  $h_*$  at GW production, red-shifted to today, is

$$h_* = 16.5 \times 10^{-3} \text{mHz} \left(\frac{T_*}{100 \text{ GeV}}\right) \left(\frac{g_*}{100}\right)^{1/6}. \quad (3.9)$$

The SW contribution is given by [63]:

$$h^2 \Omega_{\text{SW}}(f) = 2.65 \times 10^{-6} \left(\frac{H_*}{\beta}\right) \left(\frac{\kappa_v \alpha}{1 + \alpha}\right)^2 \left(\frac{100}{g_*}\right)^{1/3} v_w S_{\text{SW}}(f)$$

where  $\kappa_v$  is the fraction of vacuum energy that is converted to bulk motion of the fluid, and the spectral shape

$$S_{\text{SW}}(f) = \left(\frac{f}{f_{\text{SW}}}\right)^3 \left(\frac{7}{4 + 3(f/f_{\text{SW}})^2}\right)^{7/2} \quad (3.10)$$

with the peak frequency

$$f_{\text{SW}} = 1.008 \times \frac{2}{\sqrt{3}v_w} \left(\frac{\beta}{H_*}\right) h_*. \quad (3.11)$$

The MHD turbulence contribution is given by [68, 71]:

$$h^2 \Omega_{\text{MHD}}(f) = 3.35 \times 10^{-4} \left(\frac{H_*}{\beta}\right) \left(\frac{\kappa_{\text{MHD}} \alpha}{1 + \alpha}\right)^{3/2} \left(\frac{100}{g_*}\right)^{1/3} v_w S_{\text{MHD}}(f),$$

where  $\kappa_{\text{MHD}}$  is the fraction of vacuum energy that is transformed into MHD turbulence, and the spectral shape can be found analytically

$$S_{\text{MHD}}(f) = \frac{(f/f_{\text{MHD}})^3}{[1 + (f/f_{\text{MHD}})]^{11/3} (1 + 8\pi f/h_*)} \quad (3.12)$$

with the peak frequency measured today is

$$f_{\text{MHD}} = 0.935 \left(\frac{3.5}{2v_w}\right) \left(\frac{\beta}{H_*}\right) h_*. \quad (3.13)$$

In calculating the GW signal, we need to know the following quantities:

- The ratio  $\alpha$  of vacuum energy density released in the PT to that of the radiation bath.
- The rate of the PT,  $\beta/H_*$ . The smaller  $\beta/H_*$ , the stronger the PT. From the bubble nucleation rate  $\Gamma(t) = A(t)e^{-S_E(t)}$  [72], with  $A(t)$  the amplitude and  $S_E$  the Euclidean action of a critical bubble, we have:

$$\beta \equiv - \left. \frac{dS_E}{dt} \right|_{t=t_*} = TH_* \left. \frac{dS_E}{dT} \right|_{T=T_*}, \quad (3.14)$$

where we have assumed the nucleation temperature  $T_n \simeq T_*$  (or equivalently  $t_n \simeq t_*$  with  $t_n$  and  $t_*$  respectively the time for bubble nucleation and GW production). For a very strong FOPT, a potential barrier between the symmetric and broken phases may still be present at  $T = 0$ . Then we need to modify the above calculation for  $\beta$  as follows:

$$\beta/H_* = T \sqrt{\left. \frac{d^2 S_E(T)}{dT^2} \right|_{T=T_m}}, \quad (3.15)$$

where  $T_m$  corresponds to  $\left. \frac{dS_E(T)}{dT} \right|_{T=T_m} = 0$ , and in this case we shall assume  $T_* \simeq T_m$  (see *e.g.* Ref. [73] for a detailed discussion).

- The latent heat fractions  $\kappa$  for each of the three processes. For the case of runaway bubbles in a plasma, we have

$$\kappa_\phi = \frac{\alpha - \alpha_\infty}{\alpha}, \quad \kappa_v = \frac{\alpha_\infty}{\alpha} \kappa_\infty, \quad \kappa_{\text{MHD}} = \epsilon \kappa_v, \quad (3.16)$$

where  $\epsilon$  is the fraction of bulk motion which is turbulent, and is found to be at most (5% – 10%) [63]. To be concrete we choose  $\epsilon = 0.1$  in this paper. We also have:

$$\kappa_\infty \equiv \frac{\alpha_\infty}{0.73 + 0.083\sqrt{\alpha_\infty} + \alpha_\infty}, \quad (3.17)$$

$$\text{with } \alpha_\infty \simeq \frac{30}{24\pi^2} \frac{\sum_i c_i \Delta m_i^2}{g_* T_*^2}. \quad (3.18)$$

In Eq. (3.18), the sum runs over all particles  $i$  that are light in the initial phase and heavy in the final phase.  $\Delta m_i^2$  is the squared mass difference in the two phases.  $c_i = N_i (N_i/2)$  for bosons (fermions) with  $N_i$  the degrees of freedom for the particle [74].

- The bubble wall velocity  $v_w$  in the rest frame of the fluid away from the bubble. A conservative estimate for  $v_w$  is given by [75]

$$v_w = \frac{1/\sqrt{3} + \sqrt{\alpha^2 + 2\alpha/3}}{1 + \alpha} \quad (3.19)$$

- The relativistic degrees of freedom  $g_*$  at the time of the PT, which is taken to be the SM contribution of 106.75 plus an additional 1 from the ALP.

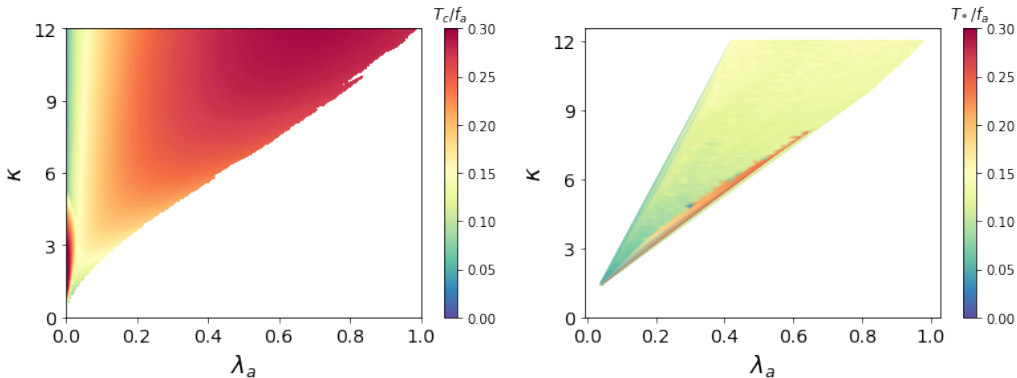


**Figure 3.** Critical temperature  $T_c$  (left) and GW emission temperature  $T_*$  (right) in units of  $f_a$  in the parameter space of  $(\kappa, \lambda_a)$ . Here we have fixed  $f_a = 10^7$  GeV.

### 3.4 Critical temperature

For the calculation of the PT and associated GW production, we take  $f_a$ ,  $\kappa$  and  $\lambda_a$  as the only free parameters in the scalar potential (2.1). Below the scale  $f_a$ , we only have the SM Higgs in the scalar sector, apart from the superlight ALP  $a$ . The value of  $\lambda_a$ , as well as the other relevant coupling constants appearing in Eqs. (2.8) and (2.9), at a high energy scale  $\Lambda < f_a$  can be obtained by running the SM renormalization group equations up to the scale  $\Lambda$  [76]. We will consider values  $f_a \leq 10^8$  GeV, as the SM vacuum becomes unstable for  $\Lambda \gtrsim 10^8$  GeV [77]. Here we have adopted the current best-fit top quark mass  $m_t = 173.0$  GeV [78]. Similarly, we take  $f_a \geq 10^3$  GeV, because for  $f_a$  comparable to (or smaller than) the Higgs mass, the LHC Higgs data impose stringent constraints on the coupling  $\kappa$  (see Section 5).

Fixing  $f_a = 10^7$  GeV, we scan the two parameters  $\kappa$  and  $\lambda_a$ . The critical temperature is shown in the left panel of Fig. 3, in units of  $f_a$ . It can be seen that in the region of interest  $T_c \lesssim 0.3f_a$ , for both type-A and type-B FOPTs. Consequently, the bubble nucleation temperature  $T_n$  is bounded by  $T_n \lesssim 0.3f_a$ .

### 3.5 Bubble nucleation

For the parameter space where there is a valid  $T_c$ , bubble nucleation will happen when  $T < T_c$ , i.e., when the two local minima become non-degenerate. Note that in our model, for both type-A or type-B transitions, the potential barrier does not vanish in the limit of  $T \rightarrow 0$ , indicating a strong FOPT, in which case the action has a minimum at  $T \in (0, T_c)$ .

We find that the quantum tunneling always dominates the nucleation process over the thermally-induced tunneling. The nucleation temperature  $T_n$  is estimated by the condition:

$$\frac{\Gamma(T_n)}{H(T_n)^4} = 1, \quad (3.20)$$

where the Hubble constant is given by [73]:

$$H(T) = \frac{\pi T^2}{3M_{\text{Pl}}} \sqrt{\frac{g_*}{10}}. \quad (3.21)$$

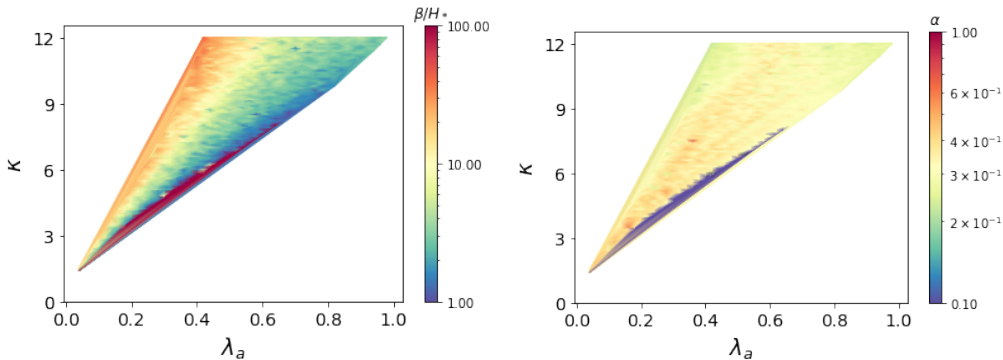


**Figure 4.**  $\beta/H_*$  (left) and  $\alpha$  (right) evaluated at  $T_*$ , for  $f_a = 10^7$  GeV.

A valid solution for  $T_n$  from Eq. (3.20) indicates that the nucleation process will happen, and the majority of the GW signal is produced at  $T_* \simeq T_n$ . We need to use Eq. (3.15) to compute  $\beta/H_*$  and  $T_*$ . The result for the nucleation temperature  $T_*$  is shown in the right panel of Fig. 3, for the specific value of  $f_a = 10^7$  GeV. It is clear from Fig. 3, that the  $T_*$  region is a subset of the FOPT region. Furthermore, the whole  $T_*$  region lies in the type-B sector. The whole parameter space of  $(\kappa, \lambda_a)$  of type-A (the darker gray region in the right panel of Fig. 3) cannot produce a valid  $T_n$ , therefore for a detectable GW signal, the FOPT must be of type-B.

The two important parameters for computing the GW signal,  $\beta/H_*$  and  $\alpha$ , are then evaluated at  $T_*$ . We show the results of these two parameters in the parameter space  $(\kappa, \lambda_a)$  for the case of  $f_a = 10^7$  GeV in Fig. 4.  $\beta/H_*$  is in the range from 1 to 100, and  $\alpha$  is of order 0.1 in most of the parameter space. In other words, the GWs are produced in the radiation-domination era after reheating.

### 3.6 Detection prospects

We have assumed that the majority of the GW signal is produced at  $T_* \simeq T_n$ . As all three GW contributions scale as inverse powers of  $\beta/H_*$ ,

$$h^2\Omega_\phi \propto \left(\frac{\beta}{H_*}\right)^{-2}, \quad h^2\Omega_{\text{SW}} \propto \left(\frac{\beta}{H_*}\right)^{-1}, \quad h^2\Omega_{\text{MHD}} \propto \left(\frac{\beta}{H_*}\right)^{-1}, \quad (3.22)$$

it is expected that a relatively large GW signal can be emitted in the small- $\beta/H_*$  region.

We compute the three different components of GW signals from bubble wall collision in Eq. (3.7), SW in the plasma in Eq. (3.10) and MHD turbulence in Eq. (3.12). The total contribution can be calculated by summing them up directly, given in Eq. (3.6), as a function of frequency  $f$ . Our numerical calculations reveal that for the configurations with  $h^2\Omega_{\text{GW}} \gtrsim 10^{-10}$  the bubble wall collision dominates the GW contributions, whereas when  $h^2\Omega_{\text{GW}} \lesssim 10^{-10}$ , the SW and MHD components also contribute sizeably to the total GW signal, as indicated by the shape of the  $h^2\Omega_{\text{GW}}$  curves in Fig. 5.

In Fig. 5, we show the prospects of future GW experiments TianQin [22], Taiji [23], LISA [24, 25], ALIA [26], MAGIS [27], DECIGO [28], BBO [30], aLIGO [29], aLIGO+ [21],

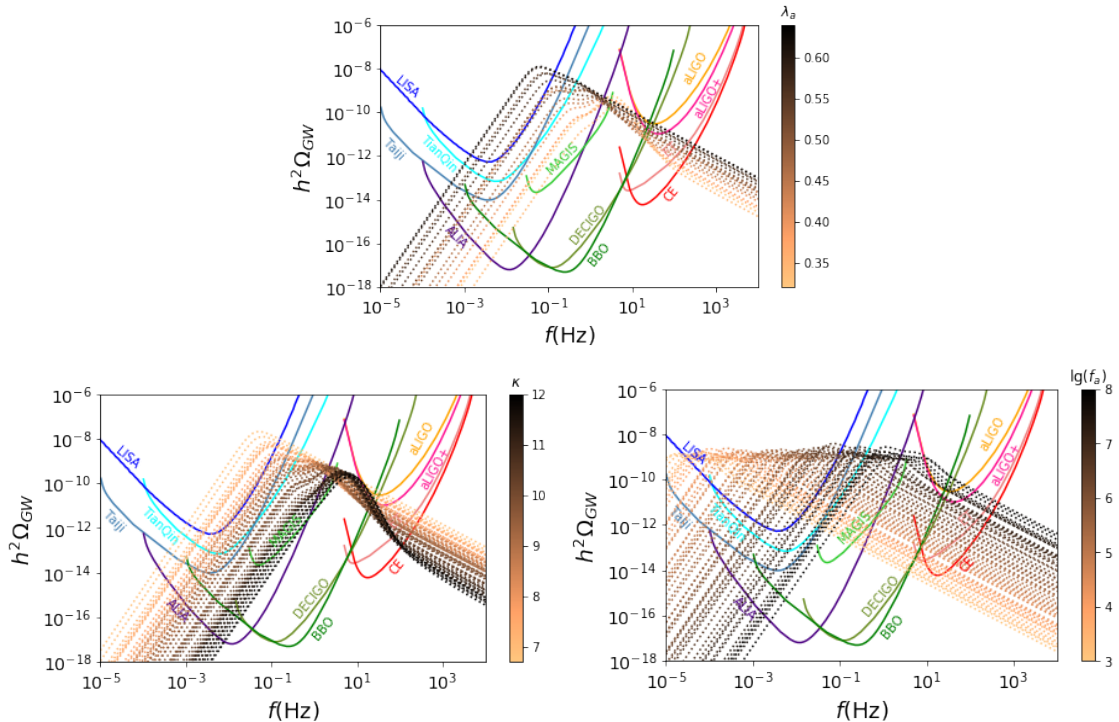


**Figure 5.** The prospects of GW experiments TianQin [22], Taiji [23], LISA [24, 25], ALIA [26], MAGIS [27], DECIGO [28], BBO [30], aLIGO [29], aLIGO+ [21], ET [32] and CE [31], and the curves of GW strength  $h^2\Omega_{\text{GW}}(f)$  as functions of the three parameters  $f_a$ ,  $\kappa$  and  $\lambda_a$  in the ALP model. In the upper panel, we have fixed  $f_a = 10^7$  GeV and  $\kappa = 8.00$  and vary  $\lambda_a$  from 0.320 to 0.640; in the lower left panel  $f_a = 10^7$  GeV and  $\lambda_a = 0.500$  with  $\kappa$  varying from 6.70 to 12.00; in the lower right panel  $\kappa = 8.00$  and  $\lambda_a = 0.500$  with  $f_a$  from  $10^3$  GeV to  $10^8$  GeV.

ET [32] and CE [31] for comparison. To see the dependence of the GW signal on the parameters  $f_a$ ,  $\kappa$  and  $\lambda_a$ , let us first fix  $f_a = 10^7$  GeV and  $\kappa = 8.00$  and vary the quartic coupling  $\lambda_a$  from 0.320 to 0.640. The corresponding GW signal  $h^2\Omega_{\text{GW}}$  is shown in the upper panel of Fig. 5, as a function of the frequency  $f$ . It is obvious that within the  $T_*$  region the configurations with larger  $\lambda_a$  tend to produce a larger GW signal with a relatively small peak frequency, which is preferred by the space-based experiments. Likewise, when we fix  $f_a = 10^7$  GeV and  $\lambda_a = 0.500$ , the configurations with a smaller  $\kappa$  tend to produce a strong GW signals at a smaller peak frequency, as shown in the lower left panel of Fig. 5, which could even be probed at LISA [24, 25]. When  $\kappa$  and  $\lambda_a$  are fixed, e.g.  $\kappa = 8.00$  and  $\lambda_a = 0.500$ , a larger  $f_a$  tends to produce a GW signal with a larger peak frequency, as seen in the lower right panel of Fig. 5. However the magnitude of the total GW strength does not change much for various  $f_a$  values.

The GW prospects in the two-dimensional plane of  $\kappa$  and  $\lambda_a$  are shown in Fig. 6 for the benchmark values of  $f_a = 10^{3,4,5,6,7,8}$  GeV. For the sake of clarity, we show only the sensitivity regions for three selected GW experiments: LISA [24, 25], BBO [30] and aLIGO+ [21].

The current and future GW observations are largely complementary to each other,

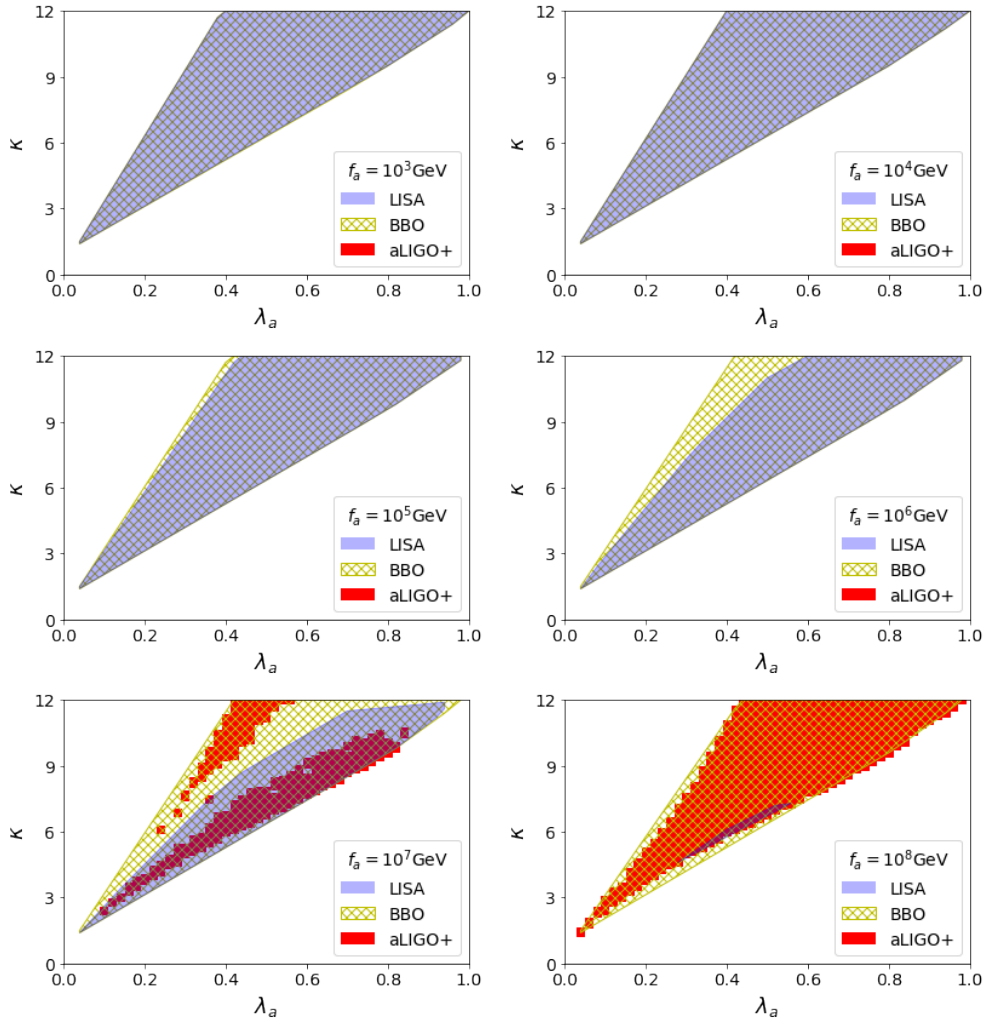


**Figure 6.** GW prospects of LISA [24, 25], BBO [30] and aLIGO+ [21] in the parameter space of  $(\kappa, \lambda_a)$ , with  $f_a = 10^{3,4,5,6,7,8}$  GeV as indicated in the plots.

i.e. TianQin [22], Taiji [23], LISA [24, 25] and ALIA [26] are more sensitive to the GWs with a comparatively lower frequency and thus a smaller  $f_a$ ; aLIGO [29], aLIGO+ [21], ET [32] and CE [31] could probe the GWs with a higher frequency and thus larger  $f_a$ , while MAGIS [27], DECIGO [28] and BBO [30] are able to cover the frequency range in between. This is explicitly illustrated in Fig. 7, with the benchmark values of  $\kappa = 8.00$  and  $\lambda_a = 0.500$ . We use the power-law integrated sensitivity curves for future GW experiments, as described in Appendix A. Although the GW in the ALP model do not involve directly the ALP particle  $a$ , the future GW observations could definitely probe a broad range of the decay constant  $f_a$ , which largely complements the low-energy, high-energy, astrophysical and cosmological constraints and prospects on the  $f_a$  parameter, as detailed in Section 4. For related discussions on the GW prospects from the ALP field itself, see e.g. Refs. [79–81].

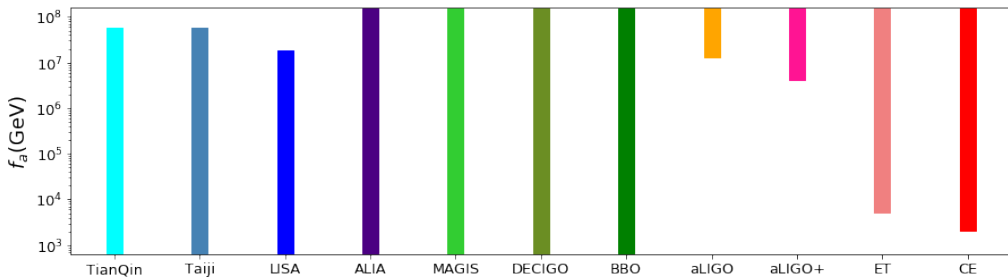


**Figure 7.** GW prospects of the  $f_a$  ranges in the experiments TianQin [22], Taiji [23], LISA [24, 25], ALIA [26], MAGIS [27], DECIGO [28], BBO [30], aLIGO [29], aLIGO+ [21], ET [32] and CE [31]. We have fixed  $\kappa = 8.00$  and  $\lambda_a = 0.500$ .

## 4 Comparison with other ALP constraints

As shown in Figs. 5, 6 of Section 3, the current and future GW observations could probe a broad region of the parameter space in the ALP model. In particular, the scale  $f_a$  could be probed in the range of  $(10^3 - 10^8)$  GeV in the future GW observations, as collected in Fig. 7. At the low-energy scale, all the couplings of ALP to the SM particles are inversely proportional to powers of the decay constant  $f_a$  [see e.g. Eq. (4.1) and (4.5)]; thus it is expected that the GW observations are largely complementary to the laboratory, astrophysical and cosmological constraints on the couplings of  $a$  to the SM particles. For the sake of simplicity, we consider only the effective CP-conserving couplings of ALP to photon ( $g_{a\gamma\gamma}$ ), electron ( $g_{aee}$ ) and nucleons ( $g_{aNN}$ ). It is also possible that ALP couples to other SM particles like the muon and tau and other gauge bosons (gluons,  $W$  and  $Z$  boson), and we can have even the CP-violating couplings of ALP to the SM particles [33, 82, 86]. See e.g. Refs. [19, 82] for more details. In addition, if the ALP couples to muon and photon [83–86] or has flavor violating coupling to muon and tau [87], it could in principle explain the muon  $g - 2$  anomaly.

### 4.1 Low-energy effective couplings of ALP

The ALP  $a$  does not couple directly to the SM Higgs or the real scalar  $\phi$  in the potential (2.1). The low-energy couplings of ALP to the SM particles can be induced at dimension-5 or higher. For instance, we can write the effective couplings of  $a$  to the SM photon and fermions  $f$  in the form of

$$\mathcal{L}_a = -\frac{C_{a\gamma}\alpha_{\text{EM}}}{8\pi f_a} a F_{\mu\nu} \tilde{F}^{\mu\nu} + \frac{\partial_\mu a}{2f_a} \sum_f C_{af} (\bar{f} \gamma^\mu \gamma^5 f), \quad (4.1)$$

with  $F_{\mu\nu}$  being the electromagnetic field strength tensor and  $\tilde{F}^{\mu\nu}$  its dual,  $\alpha_{\text{EM}}$  the fine-structure constant,  $C_{a\gamma}$  and  $C_{af}$  model-dependent coefficients. Generally speaking, these coefficients are of order one for the QCD axion. Setting the model-dependent coefficients  $C_i$  to one for simplicity, we rewrite the couplings in Eq. (4.1) as

$$\mathcal{L}_a = -\frac{g_{a\gamma\gamma}}{4} a F_{\mu\nu} \tilde{F}^{\mu\nu} - a \sum_f g_{aff} (i \bar{f} \gamma^5 f), \quad (4.2)$$

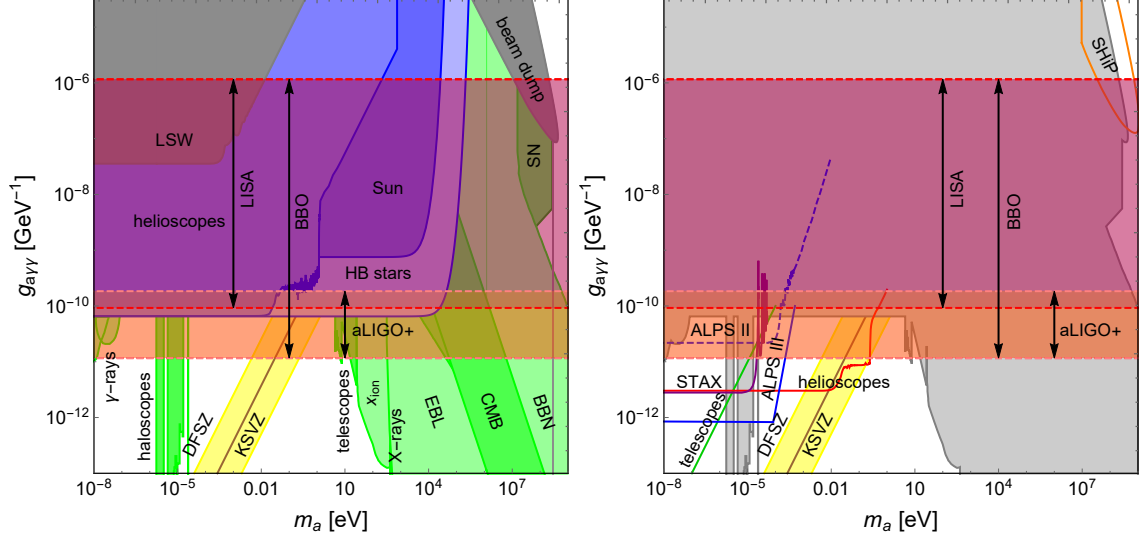


**Figure 8.** Complementarity of the GW prospects of  $g_{a\gamma\gamma}$  and the laboratory, astrophysical and cosmological constraints on the ALP mass  $m_a$  and the coupling to photon  $g_{a\gamma\gamma}$ . The GW prospects of  $g_{a\gamma\gamma}$  are shown in red (BBO [30]), purple (LISA [24, 25]) and orange (aLIGO+ [21]), with dashed border lines. The current constraints are collected in the left panel, including those from the LSW experiments [122–128], beam-dump experiments [142–146], helioscopes [103–112], the observations of Sun [99], HB stars [100] and SN1987A (labelled as “SN”) [101], telescope [93, 94] and haloscope [116–119] searches of ALP cold DM, and the cosmological constraints from BBN, CMB, EBL, x-rays,  $\gamma$ -rays,  $x_{\text{ion}}$  [92]. In the right panel, all the current limits are shown in gray, and we emphasize the future prospects from telescope observations (green line) [95], the helioscope experiments (red line) [113–115], the LSW experiments ALPS II (dashed blue line) [129], ALPS III (solid blue line) [130], STAX (solid purple line) [131] and SHiP (solid orange line) [148]. All the regions above the lines are probable in these experiments. In both the panels we also show the parameter space for the DFSZ (yellow region) [88, 89] and KSVZ axions (brown line) [90, 91]. The limits and prospects are adapted from [19]. See text for more details.

with  $m_f$  is the corresponding fermion mass and the effective couplings are related to the high scale  $f_a$  via

$$g_{a\gamma\gamma} = \frac{\alpha_{\text{EM}}}{2\pi f_a}, \quad g_{aff} = \frac{m_f}{f_a}. \quad (4.3)$$

Then the GW prospects of  $f_a$  in Fig. 7 can be used to probe the effective couplings  $g_{a\gamma\gamma}$ ,  $g_{aee}$  and  $g_{aNN}$ .

## 4.2 Coupling to photon

Following Ref. [19], all the current constraints on the coupling of ALP to photon  $g_{a\gamma\gamma}$  are collected in the left panel of Fig. 8, while the future laboratory and astrophysical prospects are shown in the right panel of Fig. 8. In the two panels we also show the parameter space for the DFSZ [88, 89] and KSVZ [90, 91] axions, indicated respectively by the yellow region and brown line. The various constraints are explained below:

- Given the coupling  $g_{a\gamma\gamma}$ , the ALP decays into two photons in the early universe, depending largely on its mass  $m_a$  and the magnitude of  $g_{a\gamma\gamma}$ . Consequently, if the

decay of ALP is earlier than the decoupling of cosmic microwave background (CMB), the photons from ALP decay would potentially distort the CMB spectrum and also affect the big bang nucleosynthesis (BBN) [92]. The monochromatic photon lines from axion/ALP decay are also constrained by the flux of extragalactic background light (EBL) and direct searches in X-rays and  $\gamma$ -rays [92]. Furthermore, the photons might also change the history of Hydrogen ionisation fraction ( $x_{\text{ion}}$ ) [92]. All the limits from CMB, BBN, EBL, X-rays,  $\gamma$ -rays and  $x_{\text{ion}}$  are shown in greenish color in the left panel of Fig. 8.

- Assuming ALPs account for all the cold DM, the regions labelled as “telescopes” in the left panel of Fig. 8 have been excluded by the direct decaying DM searches in galaxies [93, 94]. It is promising that future telescopes could probe a coupling down to [95]

$$g_{a\gamma\gamma} \sim (10^{-12} \text{ GeV}^{-1}) \times \left( \frac{m_a}{10^{-6} \text{ eV}} \right) \left( \frac{d}{2 \text{ kpc}} \right)^{1/2} \quad \text{for } 10^{-7} \text{ eV} \lesssim m_a \lesssim 10^{-4} \text{ eV}. \quad (4.4)$$

Taking the distance of ALP source to be  $d \simeq 2 \text{ kpc}$ , the future sensitivity could go down to  $g_{a\gamma\gamma} \sim 10^{-13} \text{ GeV}^{-1}$ . This is shown as the green line in the right panel of Fig. 8.

- As a result of the coupling  $g_{a\gamma\gamma}$ , the ALP can be produced and emitted copiously from the dense stellar cores, thus affecting the stellar evolution [96–98]. A large parameter space of  $m_a$  and  $g_{a\gamma\gamma}$  has been excluded by the solar neutrino flux and helioseismology [99], the ratio of horizontal branch (HB) to red giants in globular clusters [100], and the SN1987A neutrino data [101], which are labelled respectively as “Sun”, “HB stars” and “SN” in the left panel of Fig. 8.
- In presence of an electromagnetic field, the ALP can be converted to a photon through the  $a\gamma\gamma$  coupling in Eq. (4.2) [102]. The axion helioscope experiments Brookhaven [103], SUMICO [104–106] and CAST [107–112] aim to detect X-rays from the  $a - \gamma$  conversion in the Sun; no signal has been found and these helioscope data can be used to set limits on the coupling  $g_{a\gamma\gamma}$ , labelled as “helioscopes” in the left panel of Fig. 8. The future experiments TASTE [113] and IAXO [114, 115] could improve current constraints by over one order of magnitude, shown as the solid red line in the right panel of Fig. 8.
- In a static magnetic field, ALP DM in the  $\sim 10^{-6} \text{ eV}$  mass range can be converted into a microwave photon [102]. Narrow regions around this range has been excluded by the ADMX experiment [116–119], labelled as “haloscopes” in the left panel of Fig. 8. It is expected that the future stages of ADMX could probe a very narrow range around  $m_a \sim 10 \mu\text{eV}$  [120], which is not shown in the right panel of Fig. 8. The ABRACADABRA experiment can detect a light ALP with mass  $10^{-14} \text{ eV} \lesssim m_a \lesssim 10^{-6} \text{ eV}$  and coupling down to  $g_{a\gamma\gamma} \sim 10^{-19} \text{ GeV}^{-1}$  [121], not shown in the right panel of Fig. 8.

- The light-shining-through-wall (LSW) experiments provide the most stringent laboratory constraints on the coupling  $g_{a\gamma\gamma}$  for a broad range of ALP mass  $m_a$ . In such experiments, ALPs can be produced in magnetic fields from intense photon sources and convert back into photons. The LSW limits from BRFT [122], BMV [123], GammaV [124], LIPPS [125], ALPS [126], OSQAR [127] and CROWS [128] are collectively shown in the left panel of Fig. 8. The LSW limits could be further improved by up to four orders of magnitude in the experiments ALPS II [129], ALPS III [130] and STAX [131], as indicated by the dashed blue line, solid blue line and solid purple line in the right panel of Fig. 8. There are also some ALP constraints from the polarization experiment PVLAS [122, 132–134] and the searches of 5th force [135–141], which are however weaker and thus not shown in Fig. 8.
- In the beam-dump experiments, ALPs can be produced off photons. The limits on  $g_{a\gamma\gamma}$  from the experiments CHARM [142], E137 [143] E141 [144] and NuCal [145, 146] are comparatively weaker than those from the astrophysical observations above, excluding a region  $g_{a\gamma\gamma} \gtrsim 10^{-7} \text{ GeV}^{-1}$  for ALP mass  $m_a \sim (\text{MeV} - \text{GeV})$ , as shown in Fig. 8. The future experiment SHiP [147, 148] will extend the exclusion regions to a higher  $m_a$ , but not push to a smaller coupling  $g_{a\gamma\gamma}$  [149], as indicated in the right panel of Fig. 8. The projected limit from NA62 is expected to be weaker and thus not shown in Fig. 8 [150].

For sufficiently small  $g_{a\gamma\gamma}$ , the ALP might be long-lived at the high-energy colliders, thus decaying outside the detectors. There have been searches of single photon plus missing transverse energy  $e^+e^- \rightarrow \gamma + \cancel{E}_T$  at LEP [151–154] and  $pp \rightarrow \gamma + \cancel{E}_T$  at LHC [155–158]. Similarly, there are also searches of radiative decays of Upsilon mesons  $\Upsilon \rightarrow \gamma + \cancel{E}_T$  at CLEO [159] and BaBar [160], which can be used to set limits on the ALP coupling  $g_{a\gamma\gamma}$ . If the ALP decays promptly in the detectors, then we have the signatures of three photons  $e^+e^-$ ,  $p\bar{p}$ ,  $pp \rightarrow \gamma + a \rightarrow \gamma\gamma\gamma$  at LEP [161, 162], Tevatron [163] and LHC [164, 165]. These limits could be improved by one to two orders of magnitude at future colliders such as Belle II [166], ILC [167], FCC-ee [168] and later stages of LHC [169, 170]. Benefiting from the large proton number in heavy ions, the photon-photon luminosity can be largely enhanced in heavy-ion collisions compared to proton-proton colliders, and the current LHC bounds on  $g_{a\gamma\gamma}$  can be improved by two orders of magnitude in ultra-peripheral heavy-ion collisions [171]. However, even at future colliders, the prospective limits are still too weak, at the level of  $g_{a\gamma\gamma} \gtrsim 10^{-5} \text{ GeV}^{-1}$  [169–171], and hence, not shown in Fig. 8. More collider constraints on the coupling  $g_{a\gamma\gamma}$  can be found e.g. in Refs. [33, 172].

At dimension-6 and dimension-7, we have the effective operators [33, 82, 86]

$$\mathcal{L}_a \supset \frac{C_6}{f_a^2} (\partial_\mu a)(\partial^\mu a)(H^\dagger H) + \frac{C_7}{f_a^3} (\partial^\mu a)(H^\dagger i D_\mu H)(H^\dagger H) \quad (4.5)$$

with  $C_{6,7}$  the dimensionless Wilson coefficients and  $D_\mu$  the covariant derivative for the SM Higgs doublet. These operators incorporate the couplings of ALP to the SM Higgs (and  $Z$  boson), in the form of  $haa$  and  $haZ$ , which induce exotic decays of SM Higgs, i.e.  $h \rightarrow aa$  and  $h \rightarrow aZ$  with the ALPs decaying further into two photons  $a \rightarrow \gamma\gamma$  [82, 86]. In principle

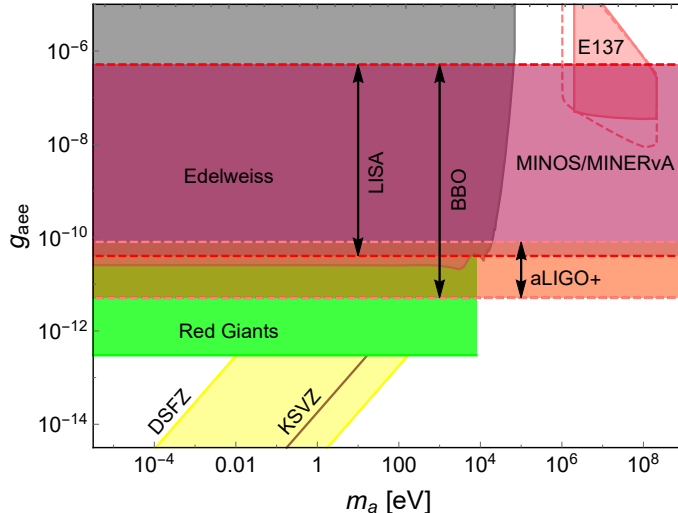


**Figure 9.** Complementarity of the GW prospects of  $g_{aee}$  and the laboratory and astrophysical constraints on the ALP mass  $m_a$  and the coupling to electron  $g_{aee}$ . The GW prospects of  $g_{aee}$  are shown in red (BBO [30]), purple (LISA [24, 25]) and orange (aLIGO+ [21]), with dashed border lines. The constraints include those from EDELWEISS (gray) [175], Red Giants (green) [182], and beam-dump experiment E137 (pink) [143]. The dashed gray line indicates the prospect at MINOS/MINERvA [183]. We also show the parameter space for the DFSZ (yellow region) [88, 89] and KSVZ axions (brown line) [90, 91]. See text for more details.

we can set limits on  $g_{a\gamma\gamma}$  from the searches of exotic decays of SM Higgs  $h \rightarrow aa \rightarrow 4\gamma$  and  $h \rightarrow aZ \rightarrow \gamma\gamma\ell^+\ell^-$  (with  $\ell = e, \mu$ ), which however depend largely on the coefficients  $C_{6,7}$  in Eq. (4.5), thus we do not include them in Fig. 8.

By using the relation in Eq. (4.3), the GW prospects of  $f_a$  in BBO [30], LISA [24, 25] and aLIGO+ [21] can be converted to sensitivities of the effective coupling  $g_{a\gamma\gamma}$  which does not depend on the ALP mass  $m_a$  and are shown respectively as the red, purple and orange horizontal bands in Fig. 8, with dashed border lines. When combined, these GW observations are sensitive to the range of

$$10^{-11} \text{ GeV}^{-1} \lesssim g_{a\gamma\gamma} \lesssim 10^{-6} \text{ GeV}^{-1}. \quad (4.6)$$

As shown in Fig. 8, some of the regions within this range of  $g_{a\gamma\gamma}$  have been excluded by the astrophysical and cosmological observations and laboratory experiments, while some are still unconstrained. If a GW signal could be found in the near future, then we would expect a positive signal in the future searches of ALPs, for instance in the telescope [95], helioscopes [113–115] searches, the LSW experiments ALPS II [129], ALPS III [130] and STAX [131], ADMX [120], ABRACADABRA [121], and the beam-dump experiments like SHiP [148], as shown in the right panel of Fig. 8, assuming that the GW signal is indeed from the PT in the ALP model.

### 4.3 Coupling to electron

All the astrophysical and laboratory constraints on the coupling  $g_{aee}$  of ALP to electron are collected in Fig. 9. In this figure we also show the parameter space of the DFSZ [88, 89]

and KSVZ [90, 91] axions. As for the case of  $g_{a\gamma\gamma}$ , the exotic SM Higgs decays  $h \rightarrow aa$  and  $h \rightarrow aZ$  can not be used to set robust limits on the coupling  $g_{ae}$ , as they depend also on the coefficients  $C_{6,7}$  in Eq. (4.5). The other constraints are described below:

- ALPs can be produced by bremsstrahlung and Compton effects in the Sun, and model-independent constraints on the mass  $m_a$  and coupling  $g_{aee}$  have been imposed by the searches of electron recoil in the low-background experiments Derbin [173], XMASS [174] and EDELWEISS [175]. The limit from EDELWEISS is the most stringent, which is shown as the gray region in Fig. 9. There are also constraints from CoGeNT [176] and CDMS [177] on ALP DM in local galaxies, which exclude however a much narrower region of  $g_{aee}$ . The limits on  $g_{aee}$  from CUORE [178], Derbin [179] and Borexino [180] depend on the effective coupling  $g_{aNN}^{\text{eff}}$  of ALP to nucleus, thus they are not shown in Fig. 9.
- If ALP couples to electron, it will lead to extra energy loss in the astrophysical objects. The constraints from observations of solar neutrino [181] and Red Giants [182] have excluded a broad region in the parameter space of  $m_a$  and  $g_{aee}$ . We have shown the Red Giant excluded region in Fig. 9 in green, while the solar neutrino limits are comparatively much weaker.
- ALPs can be produced in the beam-dump experiments by bremsstrahlung off an incident electron beam and decay back into electron-positron pairs in the detector [183]. The region excluded by E137 [143] is shown in Fig. 9 in pink. The experiment MINOS/MINERvA could improve significantly the current limit [183], as indicated by the dashed gray line.

Given the relation in Eq. (4.3), the GW experiments BBO [30], LISA [24, 25] and aLIGO+ [21] could probe a range of

$$10^{-11.5} \lesssim g_{aee} \lesssim 10^{-6.5}. \quad (4.7)$$

A sizable fraction of the range has been excluded by the constraints from EDELWEISS [175] and Red Giants [182], with  $m_a \lesssim 10$  keV. If the GW experiments LISA and BBO could find a GW signal, then the corresponding ALP mass is expected to be heavier than roughly 10 keV, and might be tested in the MINOS/MINERvA experiment [183].

#### 4.4 Coupling to nucleon

All the limits on the effective coupling  $g_{aNN}$  of ALP to nucleon are collected in Fig. 10, including the parameter space of the DFSZ [88, 89] and KSVZ [90, 91] axions.

- In compact astrophysical objects like neutron stars and supernova cores, nucleon bremsstrahlung  $N + N \rightarrow N + N + a$  is the most effective channel to produce ALPs [184, 185], with  $N = p, n$  including both proton and neutron. The neutron star constraints on the coupling  $g_{aNN}$  can be found in e.g. [184, 186]. The limits from neutrino bursts from SN1987A are stronger, which exclude a coupling

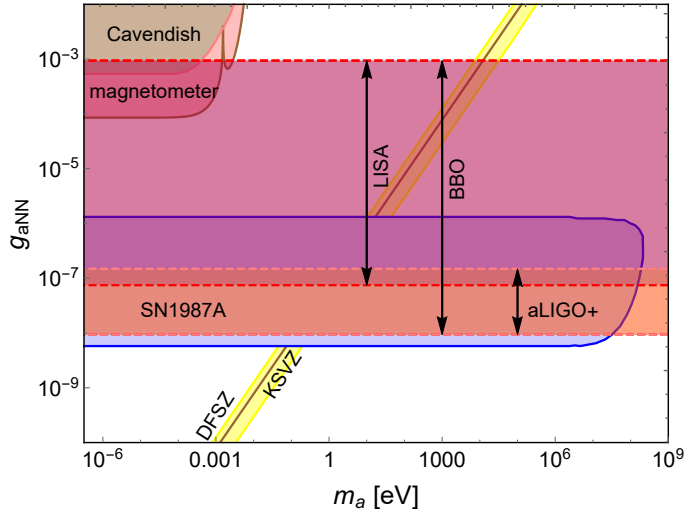


**Figure 10.** Complementarity of the GW prospects of  $g_{aNN}$  and the astrophysical constraints on the ALP mass  $m_a$  and the coupling to nucleon  $g_{aNN}$ . The GW prospects of  $g_{aNN}$  are shown in red (BBO [30]), purple (LISA [24, 25]) and orange (aLIGO+ [21]), with dashed border lines. The constraints include those from SN1987A [183] (blue), Cavendish-type experiment (brown) and magnetometer experiment (pink). We also show the parameter space for the DFSZ (yellow region) [88, 89] and KSVZ axions (brown line) [90, 91]. See text for more details.

$10^{-8} \lesssim g_{aNN} \lesssim 10^{-6}$  for  $m_a \lesssim 100$  MeV [183, 187–192], as shown in blue in Fig. 10. It is promising that the next-generation supernova observations could improve largely the limits on  $g_{aNN}$ , depending on how far the next supernova explosion is [193].

- The Yukawa couplings of ALP to nucleons could potentially cause violation of the gravitational inverse-square law, and the effective coupling  $g_{aNN}$  is thus constrained by the Cavendish-type experiment [136, 194], as shown in brown in Fig. 10. The limits from measurements of Casimir forces are comparatively weaker with  $g_{aNN} \lesssim 10^{-2.5}$  [195, 196], and are thus not shown in Fig. 10.
- Searches of new long-range spin-dependent forces between nucleons can be used to set limits on the coupling  $g_{aNN}$ . The magnetometer experiment has excluded a coupling  $g_{aNN} \gtrsim 10^{-4}$  for ALP mass  $m_a \lesssim$  meV [197], as shown in pink in Fig. 10.

The GW experiments BBO [30], LISA [24, 25] and aLIGO+ [21] could probe a range of

$$10^{-8} \lesssim g_{aNN} \lesssim 10^{-3}, \quad (4.8)$$

which is largely complementary to the supernova and laboratory constraints.

## 5 Prospects from precision Higgs data at future colliders

If the scalar  $\phi$  in the ALP model resides at the few-TeV scale, it will contribute to the trilinear coupling  $\lambda_3$  of the SM Higgs through the quartic coupling  $\kappa$ . This is obtained

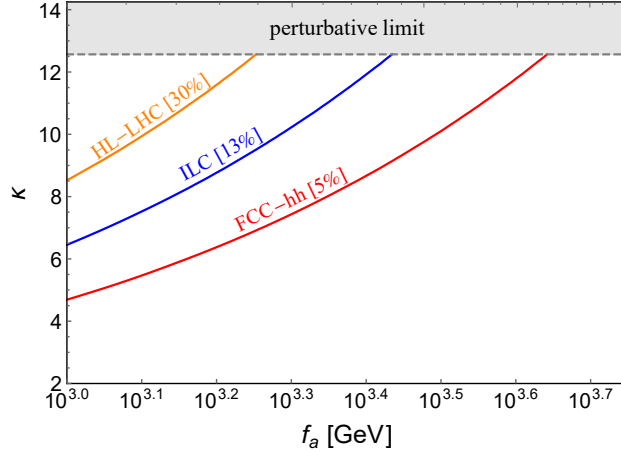


**Figure 11.** Prospects of the trilinear coupling of the SM Higgs at the confidence level of  $1\sigma$  at HL-LHC with the center-of-mass energy of  $\sqrt{s} = 14$  TeV and an integrated luminosity of  $3 \text{ ab}^{-1}$  [203–207], FCC-hh with  $\sqrt{s} = 100$  TeV and  $30 \text{ ab}^{-1}$  [208] and ILC with  $\sqrt{s} = 1$  TeV and  $2.5 \text{ ab}^{-1}$  [209, 210], as functions of the scale  $f_a$  and the coupling  $\kappa$  in the ALP model. The shaded region is excluded by the perturbative limit.

from the temperature-independent effective potential  $\mathcal{V}$  in Eq. (2.4), after integrating out the  $\phi$ -field, and reads [198]

$$\lambda_3 \simeq \lambda_3^{\text{SM}} + \frac{\kappa^3 v_{\text{EW}}^3}{24\pi^2 m_\phi^2}, \quad (5.1)$$

with the SM contribution  $\lambda_3^{\text{SM}} = m_h^2/2v_{\text{EW}}$ . It is expected that if the quartic coupling  $\lambda_a \simeq \mathcal{O}(0.1) - \mathcal{O}(1)$  as seen in Fig. 6, the mass  $m_\phi = \sqrt{4\lambda_a}f_a$  is of the same order as the scale  $f_a$ , then we can set limits on the  $f_a$  scale and  $\kappa$  by precision measurement of the trilinear SM Higgs coupling at high-energy colliders. The current Higgs pair production data at LHC lead to the limit  $-9 \lesssim \lambda_3/\lambda_3^{\text{SM}} \lesssim 15$  [199–201], which is too weak to exclude any parameter space of the ALP model. In the future hadron colliders like high-luminosity LHC (HL-LHC) and FCC-hh [202] and lepton colliders such as ILC [167], the trilinear scalar coupling can be more precisely measured, which can be used to probe the scale  $f_a$  and the quartic coupling  $\kappa$  in the ALP model. It is expected that the trilinear coupling  $\lambda_3$  can be measured up to (30% - 50%) at the confidence level of  $1\sigma$  at the HL-LHC 14 TeV with an integrated luminosity of  $3 \text{ ab}^{-1}$  [203–207]. With a larger cross section, the precision can be improved up to  $\sim 5\%$  at future 100 TeV collider FCC-hh with a luminosity of  $30 \text{ ab}^{-1}$  [208], and up to 13% at ILC 1 TeV with a luminosity of  $2.5 \text{ ab}^{-1}$  [209, 210]. All these sensitivities are shown in Fig. 11, with the benchmark value  $\lambda_a = 0.25$ . The parameter space of  $f_a$  and  $\kappa$  above these lines can be probed at future high energy colliders. which is largely complementary to the low energy axion experiments and the GW observations for TeV scale  $f_a$ .

## 6 Conclusion

In this paper we have studied the GW production due to strong FOPT in a generic axion or ALP model, where we extended the SM scalar sector by adding only a complex singlet field  $\Phi$ . The angular component of  $\Phi$  is identified as the axion or ALP field  $a$ . In the original Lagrangian, we have only a few free parameters, namely, the ALP mass  $m_a$ , the “axion decay constant”  $f_a$  and the quartic couplings  $\kappa$  and  $\lambda_a$  in the tree-level zero-temperature potential (2.1). We have explored the energy scale  $f_a$  from  $10^3$  GeV to  $10^8$  GeV for GW prospects. Our numerical calculations reveal that in the ALP model we are considering, the GW signal strength could be as large as  $h^2\Omega_{\text{GW}} \sim 10^{-8}$ , promisingly detectable at the GW experiments like BBO [30], LISA [24, 25] and aLIGO+ [21], depending on the GW frequency and the ALP model parameters. (see Figs. 5-7).

At the low energy scale, the couplings of ALP to the SM particles are universally determined by the decay constant  $f_a$ , up to some model-dependent coefficients; in other words, all the effective couplings of ALP depend inversely on the powers of  $f_a$ . Therefore, we can convert the GW prospects of  $f_a$  to the sensitivities on the effective couplings of ALP to the SM particles, independent of the ALP mass  $m_a$ . We have considered the CP-conserving couplings of ALP to photon  $g_{a\gamma\gamma}$ , to electron  $g_{aee}$  and to nucleon  $g_{aNN}$ . These couplings are tightly constrained by a large variety of laboratory experiments and astrophysical and cosmological observations, and broad regions have been excluded depending on the ALP mass  $m_a$ . The GW experiments would probe sizable regions of the unconstrained parameter space, namely,  $10^{-11} \text{ GeV}^{-1} \lesssim g_{a\gamma\gamma} \lesssim 10^{-6} \text{ GeV}^{-1}$ ,  $10^{-11.5} \lesssim g_{aee} \lesssim 10^{-6.5}$  and  $10^{-8} \lesssim g_{aNN} \lesssim 10^{-3}$ , which are largely complementary to the laboratory, astrophysical and cosmological constraints. Thus, if a GW signal is found in the future GW experiments and interpreted in the framework of axion or ALP models, it can be cross-checked in the upcoming laboratory and/or astrophysical searches of ALPs. In addition, if  $f_a$  is at the TeV scale, then the real component  $\phi$  contributes to the trilinear coupling of the SM Higgs. Thus the precision Higgs data at future hadron and lepton colliders can be used to probe the  $f_a$  and  $\kappa$  parameters in the ALP model, which complements largely the low-energy axion/ALP experiments and the GW observations.

## Acknowledgements

We thank Robert Caldwell for useful discussions and comments on the draft. B.D. also thanks Aniket Joglekar for discussion on the trilinear Higgs coupling. This work was supported by the US Department of Energy under Grant No. DE-SC0017987. Y.C.Z. is grateful to the Center for High Energy Physics, Peking University for generous hospitality where part of the work was done.

## A Power-law Integrated Sensitivity Curves

We briefly outline the procedure used to compute the power-law integrated sensitivity curves for the current and future GW experiments. For a detailed description of this method, see Ref. [211].

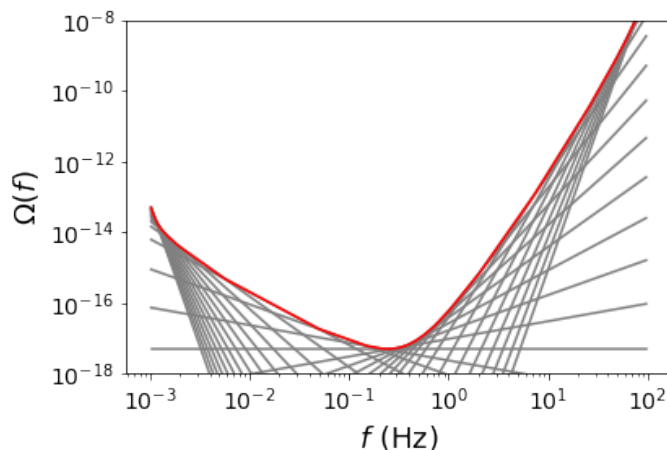


**Figure 12.** The sensitivity curves for BBO. The red curve is the power-law integrated sensitivity curve defined in Eq. (A.4); the gray curves are sensitivity curves for different power-law indices, defined in Eq. (A.3).

In the literature, the square root  $\sqrt{S_n(f)}$  of the strain power spectral density is usually given as a function of frequency, in units of  $1/\sqrt{\text{Hz}}$ . First of all, we convert it to  $\Omega_n(f)$  by

$$\Omega_n(f) = \frac{2\pi^2}{3H_0^2} f^3 S_n(f). \quad (\text{A.1})$$

Then, given a set of power-law indices  $\beta$ , e.g.  $\beta \in \{-8, -7, \dots, 7, 8\}$ , for each  $\beta$  we compute

$$\Omega_{0\beta} = \frac{\rho}{\sqrt{2T}} \left[ \int_{f_{\min}}^{f_{\max}} df \frac{(f/f_{\text{ref}})^{2\beta}}{\Omega_n^2(f)} \right]^{-1/2}, \quad (\text{A.2})$$

where  $f_{\text{ref}}$  is some reference frequency. It can be chosen arbitrarily and will not affect the result.  $\rho$  is the integrated signal-to-noise ratio and  $T$  is the observation time. Following Ref. [211], taking  $\rho = 1$  and  $T = 1$  year, we have

$$\Omega_\beta(f) = \Omega_{0\beta} \left( \frac{f}{f_{\text{ref}}} \right)^\beta. \quad (\text{A.3})$$

The power-law integrated sensitivity curve  $\Omega_{\text{PI}}(f)$  is the envelope of all the  $\Omega_\beta(f)$  curves,

$$\Omega_{\text{GW}}(f) = \max \left[ \Omega_{0\beta} \left( \frac{f}{f_{\text{ref}}} \right)^\beta \right]. \quad (\text{A.4})$$

As an explicit example, the power-law integrated curve  $\Omega_{\text{GW}}(f)$  of BBO as well as the series of  $\Omega_\beta(f)$  are presented in Fig. 12.

## References

- [1] R. D. Peccei and H. R. Quinn, Phys. Rev. Lett. **38**, 1440 (1977).

- [2] P. W. Graham, D. E. Kaplan and S. Rajendran, *Phys. Rev. Lett.* **115**, no. 22, 221801 (2015) [arXiv:1504.07551 [hep-ph]].
- [3] K. Freese, J. A. Frieman and A. V. Olinto, *Phys. Rev. Lett.* **65**, 3233 (1990).
- [4] F. C. Adams, J. R. Bond, K. Freese, J. A. Frieman and A. V. Olinto, *Phys. Rev. D* **47**, 426 (1993) [hep-ph/9207245].
- [5] R. Daido, F. Takahashi and W. Yin, *JCAP* **1705**, no. 05, 044 (2017) [arXiv:1702.03284 [hep-ph]].
- [6] J. Preskill, M. B. Wise and F. Wilczek, *Phys. Lett. B* **120**, 127 (1983).
- [7] L. F. Abbott and P. Sikivie, *Phys. Lett. B* **120**, 133 (1983).
- [8] M. Dine and W. Fischler, *Phys. Lett. B* **120**, 137 (1983).
- [9] P. Jain, *Mod. Phys. Lett. A* **20**, 1763 (2005) [hep-ph/0411279].
- [10] J. E. Kim and H. P. Nilles, *JCAP* **0905**, 010 (2009) [arXiv:0902.3610 [hep-th]].
- [11] J. E. Kim and H. P. Nilles, *Phys. Lett. B* **730**, 53 (2014) [arXiv:1311.0012 [hep-ph]].
- [12] A. Lloyd-Stubbs and J. McDonald, *Phys. Rev. D* **99**, no. 2, 023510 (2019) [arXiv:1807.00778 [hep-ph]].
- [13] R. Daido, N. Kitajima and F. Takahashi, *JCAP* **1507**, no. 07, 046 (2015) [arXiv:1504.07917 [hep-ph]].
- [14] A. De Simone, T. Kobayashi and S. Liberati, *Phys. Rev. Lett.* **118**, no. 13, 131101 (2017) [arXiv:1612.04824 [hep-ph]].
- [15] G. Ballesteros, J. Redondo, A. Ringwald and C. Tamarit, *Phys. Rev. Lett.* **118**, no. 7, 071802 (2017) [arXiv:1608.05414 [hep-ph]].
- [16] Y. Ema, K. Hamaguchi, T. Moroi and K. Nakayama, *JHEP* **1701**, 096 (2017) [arXiv:1612.05492 [hep-ph]].
- [17] R. S. Gupta, J. Y. Reiness and M. Spannowsky, arXiv:1902.08633 [hep-ph].
- [18] J. Jaeckel and A. Ringwald, *Ann. Rev. Nucl. Part. Sci.* **60**, 405 (2010) [arXiv:1002.0329 [hep-ph]].
- [19] I. G. Irastorza and J. Redondo, *Prog. Part. Nucl. Phys.* **102**, 89 (2018) [arXiv:1801.08127 [hep-ph]].
- [20] N. Aghanim *et al.* [Planck Collaboration], arXiv:1807.06209 [astro-ph.CO].
- [21] The LIGO Scientific Collaboration, LIGO DCC-T1400316 (2014).
- [22] J. Luo *et al.* [TianQin Collaboration], *Class. Quant. Grav.* **33**, no. 3, 035010 (2016) [arXiv:1512.02076 [astro-ph.IM]].
- [23] Z. K. Guo, R. G. Cai and Y. Z. Zhang, arXiv:1807.09495 [gr-qc].
- [24] H. Audley *et al.* [LISA Collaboration], arXiv:1702.00786 [astro-ph.IM].
- [25] T. Robson, N. Cornish and C. Liu, arXiv:1803.01944 [astro-ph.HE].
- [26] X. Gong *et al.*, *J. Phys. Conf. Ser.* **610**, no. 1, 012011 (2015) [arXiv:1410.7296 [gr-qc]].
- [27] J. Coleman [MAGIS-100 Collaboration], arXiv:1812.00482 [physics.ins-det].
- [28] M. Musha [DECIGO Working group], *Proc. SPIE Int. Soc. Opt. Eng.* **10562**, 105623T (2017).

- [29] [LIGO Scientific Collaboration], arXiv:1904.03187 [gr-qc].
- [30] V. Corbin and N. J. Cornish, *Class. Quant. Grav.* **23**, 2435 (2006) [gr-qc/0512039].
- [31] B. P. Abbott *et al.* [LIGO Scientific Collaboration], *Class. Quant. Grav.* **34**, no. 4, 044001 (2017) [arXiv:1607.08697 [astro-ph.IM]].
- [32] M. Punturo *et al.*, *Class. Quant. Grav.* **27**, 194002 (2010).
- [33] I. Brivio, M. B. Gavela, L. Merlo, K. Mimasu, J. M. No, R. del Rey and V. Sanz, *Eur. Phys. J. C* **77**, no. 8, 572 (2017) [arXiv:1701.05379 [hep-ph]].
- [34] M. S. Turner, *Phys. Rev. D* **55**, R435 (1997) [astro-ph/9607066].
- [35] R. Easther and E. A. Lim, *JCAP* **0604**, 010 (2006) [astro-ph/0601617].
- [36] R. Easther, J. T. Giblin, Jr. and E. A. Lim, *Phys. Rev. Lett.* **99**, 221301 (2007) [astro-ph/0612294].
- [37] L. Senatore, E. Silverstein and M. Zaldarriaga, *JCAP* **1408**, 016 (2014) [arXiv:1109.0542 [hep-th]].
- [38] M. C. Guzzetti, N. Bartolo, M. Liguori and S. Matarrese, *Riv. Nuovo Cim.* **39**, no. 9, 399 (2016) [arXiv:1605.01615 [astro-ph.CO]].
- [39] N. Bartolo *et al.*, *JCAP* **1612**, no. 12, 026 (2016) [arXiv:1610.06481 [astro-ph.CO]].
- [40] B. P. Abbott *et al.* [LIGO Scientific and Virgo Collaborations], *Phys. Rev. Lett.* **116**, no. 13, 131102 (2016) [arXiv:1602.03847 [gr-qc]].
- [41] P. S. B. Dev and A. Mazumdar, *Phys. Rev. D* **93**, no. 10, 104001 (2016) [arXiv:1602.04203 [hep-ph]].
- [42] L. Dolan and R. Jackiw, *Phys. Rev. D* **9**, 3320 (1974).
- [43] P. B. Arnold and O. Espinosa, *Phys. Rev. D* **47**, 3546 (1993) Erratum: [*Phys. Rev. D* **50**, 6662 (1994)] [hep-ph/9212235].
- [44] M. Quiros, hep-ph/9901312.
- [45] D. Curtin, P. Meade and H. Ramani, *Eur. Phys. J. C* **78**, no. 9, 787 (2018) [arXiv:1612.00466 [hep-ph]].
- [46] S. R. Coleman and E. J. Weinberg, *Phys. Rev. D* **7**, 1888 (1973).
- [47] J. Iliopoulos, C. Itzykson and A. Martin, *Rev. Mod. Phys.* **47**, 165 (1975).
- [48] E. J. Weinberg and A. q. Wu, *Phys. Rev. D* **36**, 2474 (1987).
- [49] C. Delaunay, C. Grojean and J. D. Wells, *JHEP* **0804**, 029 (2008) [arXiv:0711.2511 [hep-ph]].
- [50] C. L. Wainwright, *Comput. Phys. Commun.* **183**, 2006 (2012) [arXiv:1109.4189 [hep-ph]].
- [51] S. R. Coleman, *Phys. Rev. D* **15**, 2929 (1977) Erratum: [*Phys. Rev. D* **16**, 1248 (1977)].
- [52] A. D. Linde, *Phys. Lett.* **100B**, 37 (1981).
- [53] A. D. Linde, *Nucl. Phys. B* **216**, 421 (1983) Erratum: [*Nucl. Phys. B* **223**, 544 (1983)].
- [54] A. Kosowsky, M. S. Turner and R. Watkins, *Phys. Rev. D* **45**, 4514 (1992).
- [55] A. Kosowsky and M. S. Turner, *Phys. Rev. D* **47**, 4372 (1993) [astro-ph/9211004].
- [56] S. J. Huber and T. Konstandin, *JCAP* **0809**, 022 (2008) [arXiv:0806.1828 [hep-ph]].
- [57] A. Kosowsky, M. S. Turner and R. Watkins, *Phys. Rev. Lett.* **69**, 2026 (1992).

- [58] M. Kamionkowski, A. Kosowsky and M. S. Turner, Phys. Rev. D **49**, 2837 (1994) [astro-ph/9310044].
- [59] C. Caprini, R. Durrer and G. Servant, Phys. Rev. D **77**, 124015 (2008) [arXiv:0711.2593 [astro-ph]].
- [60] M. Hindmarsh, S. J. Huber, K. Rummukainen and D. J. Weir, Phys. Rev. Lett. **112**, 041301 (2014) [arXiv:1304.2433 [hep-ph]].
- [61] J. T. Giblin, Jr. and J. B. Mertens, JHEP **1312**, 042 (2013) [arXiv:1310.2948 [hep-th]].
- [62] J. T. Giblin and J. B. Mertens, Phys. Rev. D **90**, no. 2, 023532 (2014) [arXiv:1405.4005 [astro-ph.CO]].
- [63] M. Hindmarsh, S. J. Huber, K. Rummukainen and D. J. Weir, Phys. Rev. D **92**, no. 12, 123009 (2015) [arXiv:1504.03291 [astro-ph.CO]].
- [64] C. Caprini and R. Durrer, Phys. Rev. D **74**, 063521 (2006) [astro-ph/0603476].
- [65] T. Kahniashvili, A. Kosowsky, G. Gogoberidze and Y. Maravin, Phys. Rev. D **78**, 043003 (2008) [arXiv:0806.0293 [astro-ph]].
- [66] T. Kahniashvili, L. Campanelli, G. Gogoberidze, Y. Maravin and B. Ratra, Phys. Rev. D **78**, 123006 (2008) Erratum: [Phys. Rev. D **79**, 109901 (2009)] [arXiv:0809.1899 [astro-ph]].
- [67] T. Kahniashvili, L. Kisslinger and T. Stevens, Phys. Rev. D **81**, 023004 (2010) [arXiv:0905.0643 [astro-ph.CO]].
- [68] C. Caprini, R. Durrer and G. Servant, JCAP **0912**, 024 (2009) [arXiv:0909.0622 [astro-ph.CO]].
- [69] Y. Cui, M. Lewicki, D. E. Morrissey and J. D. Wells, Phys. Rev. D **97**, no. 12, 123505 (2018) [arXiv:1711.03104 [hep-ph]].
- [70] C. Caprini *et al.*, JCAP **1604**, no. 04, 001 (2016) [arXiv:1512.06239 [astro-ph.CO]].
- [71] P. Binetruy, A. Bohe, C. Caprini and J. F. Dufaux, JCAP **1206**, 027 (2012) [arXiv:1201.0983 [gr-qc]].
- [72] M. S. Turner, E. J. Weinberg and L. M. Widrow, Phys. Rev. D **46**, 2384 (1992).
- [73] J. Ellis, M. Lewicki and J. M. No, [arXiv:1809.08242 [hep-ph]].
- [74] J. R. Espinosa, T. Konstandin, J. M. No and G. Servant, JCAP **1006**, 028 (2010) [arXiv:1004.4187 [hep-ph]].
- [75] P. J. Steinhardt, Phys. Rev. D **25**, 2074 (1982).
- [76] H. Arason, D. J. Castano, B. Keszthelyi, S. Mikaelian, E. J. Piard, P. Ramond and B. D. Wright, Phys. Rev. D **46**, 3945 (1992).
- [77] G. Degrassi, S. Di Vita, J. Elias-Miro, J. R. Espinosa, G. F. Giudice, G. Isidori and A. Strumia, JHEP **1208**, 098 (2012) [arXiv:1205.6497 [hep-ph]].
- [78] M. Tanabashi *et al.* [Particle Data Group], Phys. Rev. D **98**, no. 3, 030001 (2018).
- [79] C. S. Machado, W. Ratzinger, P. Schwaller and B. A. Stefanek, JHEP **1901**, 053 (2019) [arXiv:1811.01950 [hep-ph]].
- [80] N. Ramberg and L. Visinelli, arXiv:1904.05707 [astro-ph.CO].
- [81] D. Croon, R. Houtz and V. Sanz, arXiv:1904.10967 [hep-ph].

- [82] M. Bauer, M. Neubert and A. Thamm, JHEP **1712**, 044 (2017) [arXiv:1708.00443 [hep-ph]].
- [83] R. Armillis, C. Coriano, M. Guzzi and S. Morelli, JHEP **0810**, 034 (2008) [arXiv:0808.1882 [hep-ph]].
- [84] P. deNiverville, H. S. Lee and M. S. Seo, Phys. Rev. D **98**, no. 11, 115011 (2018) [arXiv:1806.00757 [hep-ph]].
- [85] C. W. Chiang, M. Takeuchi, P. Y. Tseng and T. T. Yanagida, Phys. Rev. D **98**, no. 9, 095020 (2018) [arXiv:1807.00593 [hep-ph]].
- [86] M. Bauer, M. Neubert and A. Thamm, Phys. Rev. Lett. **119**, no. 3, 031802 (2017) [arXiv:1704.08207 [hep-ph]].
- [87] P. S. B. Dev, R. N. Mohapatra and Y. Zhang, Phys. Rev. Lett. **120**, no. 22, 221804 (2018) [arXiv:1711.08430 [hep-ph]].
- [88] M. Dine, W. Fischler and M. Srednicki, Phys. Lett. **104B**, 199 (1981).
- [89] A. R. Zhitnitsky, Sov. J. Nucl. Phys. **31**, 260 (1980) [Yad. Fiz. **31**, 497 (1980)].
- [90] J. E. Kim, Phys. Rev. Lett. **43**, 103 (1979).
- [91] M. A. Shifman, A. I. Vainshtein and V. I. Zakharov, Nucl. Phys. B **166**, 493 (1980).
- [92] D. Cadamuro, S. Hannestad, G. Raffelt and J. Redondo, JCAP **1102**, 003 (2011) [arXiv:1011.3694 [hep-ph]].
- [93] R. Hlozek, D. Grin, D. J. E. Marsh and P. G. Ferreira, Phys. Rev. D **91**, no. 10, 103512 (2015) [arXiv:1410.2896 [astro-ph.CO]].
- [94] B. D. Blout, E. J. Daw, M. P. Decowski, P. T. P. Ho, L. J. Rosenberg and D. B. Yu, Astrophys. J. **546**, 825 (2001) [astro-ph/0006310].
- [95] G. Sigl, Phys. Rev. D **96**, no. 10, 103014 (2017) [arXiv:1708.08908 [astro-ph.HE]].
- [96] A. Friedland, M. Giannotti and M. Wise, Phys. Rev. Lett. **110**, no. 6, 061101 (2013) [arXiv:1210.1271 [hep-ph]].
- [97] S. Aoyama and T. K. Suzuki, Phys. Rev. D **92**, no. 6, 063016 (2015) [arXiv:1502.02357 [astro-ph.SR]].
- [98] I. Domínguez, M. Giannotti, A. Mirizzi and O. Straniero, Mem. Soc. Ast. It. **88**, 270 (2017).
- [99] N. Vinyoles, A. Serenelli, F. L. Villante, S. Basu, J. Redondo and J. Isern, JCAP **1510**, no. 10, 015 (2015) [arXiv:1501.01639 [astro-ph.SR]].
- [100] A. Ayala, I. Domanguez, M. Giannotti, A. Mirizzi and O. Straniero, Phys. Rev. Lett. **113**, no. 19, 191302 (2014) [arXiv:1406.6053 [astro-ph.SR]].
- [101] E. Masso and R. Toldra, Phys. Rev. D **52**, 1755 (1995) [hep-ph/9503293].
- [102] P. Sikivie, Phys. Rev. Lett. **51**, 1415 (1983) Erratum: [Phys. Rev. Lett. **52**, 695 (1984)].
- [103] D. M. Lazarus, G. C. Smith, R. Cameron, A. C. Melissinos, G. Ruoso, Y. K. Semertzidis and F. A. Nezrick, Phys. Rev. Lett. **69**, 2333 (1992).
- [104] S. Moriyama, M. Minowa, T. Namba, Y. Inoue, Y. Takasu and A. Yamamoto, Phys. Lett. B **434**, 147 (1998) [hep-ex/9805026].
- [105] Y. Inoue, T. Namba, S. Moriyama, M. Minowa, Y. Takasu, T. Horiuchi and A. Yamamoto, Phys. Lett. B **536**, 18 (2002) [astro-ph/0204388].

- [106] Y. Inoue, Y. Akimoto, R. Ohta, T. Mizumoto, A. Yamamoto and M. Minowa, Phys. Lett. B **668**, 93 (2008) [arXiv:0806.2230 [astro-ph]].
- [107] K. Zioutas *et al.* [CAST Collaboration], Phys. Rev. Lett. **94**, 121301 (2005) [hep-ex/0411033].
- [108] S. Andriamonje *et al.* [CAST Collaboration], JCAP **0704**, 010 (2007) [hep-ex/0702006].
- [109] E. Arik *et al.* [CAST Collaboration], JCAP **0902**, 008 (2009) [arXiv:0810.4482 [hep-ex]].
- [110] S. Aune *et al.* [CAST Collaboration], Phys. Rev. Lett. **107**, 261302 (2011) [arXiv:1106.3919 [hep-ex]].
- [111] M. Arik *et al.* [CAST Collaboration], Phys. Rev. Lett. **112**, no. 9, 091302 (2014) [arXiv:1307.1985 [hep-ex]].
- [112] V. Anastassopoulos *et al.* [CAST Collaboration], Nature Phys. **13**, 584 (2017) [arXiv:1705.02290 [hep-ex]].
- [113] V. Anastassopoulos *et al.* [TASTE Collaboration], JINST **12**, no. 11, P11019 (2017) [arXiv:1706.09378 [hep-ph]].
- [114] I. G. Irastorza *et al.*, JCAP **1106**, 013 (2011) [arXiv:1103.5334 [hep-ex]].
- [115] E. Armengaud *et al.*, JINST **9**, T05002 (2014) [arXiv:1401.3233 [physics.ins-det]].
- [116] S. De Panfilis *et al.*, Phys. Rev. Lett. **59**, 839 (1987).
- [117] W. Wuensch *et al.*, Phys. Rev. D **40**, 3153 (1989).
- [118] C. Hagmann, P. Sikivie, N. S. Sullivan and D. B. Tanner, Phys. Rev. D **42**, 1297 (1990).
- [119] S. J. Asztalos *et al.* [ADMX Collaboration], Phys. Rev. Lett. **104**, 041301 (2010) [arXiv:0910.5914 [astro-ph.CO]].
- [120] G. Rybka [ADMX Collaboration], Phys. Dark Univ. **4**, 14 (2014).
- [121] Y. Kahn, B. R. Safdi and J. Thaler, Phys. Rev. Lett. **117**, no. 14, 141801 (2016) [arXiv:1602.01086 [hep-ph]].
- [122] R. Cameron *et al.*, Phys. Rev. D **47**, 3707 (1993).
- [123] C. Robilliard, R. Battesti, M. Fouche, J. Mauchain, A. M. Sautivet, F. Amiranoff and C. Rizzo, Phys. Rev. Lett. **99**, 190403 (2007) [arXiv:0707.1296 [hep-ex]].
- [124] A. S. Chou *et al.* [GammeV (T-969) Collaboration], Phys. Rev. Lett. **100**, 080402 (2008) [arXiv:0710.3783 [hep-ex]].
- [125] A. Afanasev *et al.*, Phys. Rev. Lett. **101**, 120401 (2008) [arXiv:0806.2631 [hep-ex]].
- [126] K. Ehret *et al.*, Phys. Lett. B **689**, 149 (2010) [arXiv:1004.1313 [hep-ex]].
- [127] R. Ballou *et al.* [OSQAR Collaboration], Phys. Rev. D **92**, no. 9, 092002 (2015) [arXiv:1506.08082 [hep-ex]].
- [128] M. Betz, F. Caspers, M. Gasior, M. Thumm and S. W. Rieger, Phys. Rev. D **88**, no. 7, 075014 (2013) [arXiv:1310.8098 [physics.ins-det]].
- [129] R. Bähre *et al.*, JINST **8**, T09001 (2013) [arXiv:1302.5647 [physics.ins-det]].
- [130] A. Lindner, talk given at Physics Beyond Colliders Annual Workshop, CERN, November 2017, <https://indico.cern.ch/event/644287/>.

- [131] L. Capparelli, G. Cavoto, J. Ferretti, F. Giazotto, A. D. Polosa and P. Spagnolo, *Phys. Dark Univ.* **12**, 37 (2016) [arXiv:1510.06892 [hep-ph]].
- [132] Y. Semertzidis *et al.*, *Phys. Rev. Lett.* **64**, 2988 (1990).
- [133] F. Della Valle *et al.*, *Phys. Rev. D* **90**, no. 9, 092003 (2014) [arXiv:1406.6518 [quant-ph]].
- [134] F. Della Valle, A. Ejlli, U. Gastaldi, G. Messineo, E. Milotti, R. Pengo, G. Ruoso and G. Zavattini, *Eur. Phys. J. C* **76**, no. 1, 24 (2016) [arXiv:1510.08052 [physics.optics]].
- [135] J. K. Hoskins, R. D. Newman, R. Spero and J. Schultz, *Phys. Rev. D* **32**, 3084 (1985).
- [136] D. J. Kapner, T. S. Cook, E. G. Adelberger, J. H. Gundlach, B. R. Heckel, C. D. Hoyle and H. E. Swanson, *Phys. Rev. Lett.* **98**, 021101 (2007) [hep-ph/0611184].
- [137] R. S. Decca, D. Lopez, E. Fischbach, G. L. Klimchitskaya, D. E. Krause and V. M. Mostepanenko, *Eur. Phys. J. C* **51**, 963 (2007) [arXiv:0706.3283 [hep-ph]].
- [138] A. A. Geraci, S. J. Smullin, D. M. Weld, J. Chiaverini and A. Kapitulnik, *Phys. Rev. D* **78**, 022002 (2008) [arXiv:0802.2350 [hep-ex]].
- [139] A. O. Sushkov, W. J. Kim, D. A. R. Dalvit and S. K. Lamoreaux, *Phys. Rev. Lett.* **107**, 171101 (2011) [arXiv:1108.2547 [quant-ph]].
- [140] S. Schlamminger, K.-Y. Choi, T. A. Wagner, J. H. Gundlach and E. G. Adelberger, *Phys. Rev. Lett.* **100**, 041101 (2008) [arXiv:0712.0607 [gr-qc]].
- [141] G. L. Smith, C. D. Hoyle, J. H. Gundlach, E. G. Adelberger, B. R. Heckel and H. E. Swanson, *Phys. Rev. D* **61**, 022001 (2000).
- [142] F. Bergsma *et al.* [CHARM Collaboration], *Phys. Lett.* **157B**, 458 (1985).
- [143] J. D. Bjorken *et al.*, *Phys. Rev. D* **38**, 3375 (1988).
- [144] E. M. Riordan *et al.*, *Phys. Rev. Lett.* **59**, 755 (1987).
- [145] J. Blumlein *et al.*, *Z. Phys. C* **51**, 341 (1991).
- [146] J. Blumlein *et al.*, *Int. J. Mod. Phys. A* **7**, 3835 (1992).
- [147] S. Alekhin *et al.*, *Rept. Prog. Phys.* **79**, no. 12, 124201 (2016) [arXiv:1504.04855 [hep-ph]].
- [148] M. Anelli *et al.* [SHiP Collaboration], arXiv:1504.04956 [physics.ins-det].
- [149] B. Döbrich, J. Jaeckel, F. Kahlhoefer, A. Ringwald and K. Schmidt-Hoberg, *JHEP* **1602**, 018 (2016) [*JHEP* **1602**, 018 (2016)] [arXiv:1512.03069 [hep-ph]].
- [150] <https://cds.cern.ch/record/1404985>.
- [151] G. Abbiendi *et al.* [OPAL Collaboration], *Eur. Phys. J. C* **18**, 253 (2000) [hep-ex/0005002].
- [152] A. Heister *et al.* [ALEPH Collaboration], *Eur. Phys. J. C* **28**, 1 (2003).
- [153] P. Achard *et al.* [L3 Collaboration], *Phys. Lett. B* **587**, 16 (2004) [hep-ex/0402002].
- [154] J. Abdallah *et al.* [DELPHI Collaboration], *Eur. Phys. J. C* **38**, 395 (2005) [hep-ex/0406019].
- [155] S. Chatrchyan *et al.* [CMS Collaboration], *Phys. Rev. Lett.* **108**, 261803 (2012) [arXiv:1204.0821 [hep-ex]].
- [156] G. Aad *et al.* [ATLAS Collaboration], *Phys. Rev. Lett.* **110**, no. 1, 011802 (2013) [arXiv:1209.4625 [hep-ex]].
- [157] CMS Collaboration [CMS Collaboration], CMS-PAS-EXO-12-047.

- [158] G. Aad *et al.* [ATLAS Collaboration], Phys. Rev. D **91**, no. 1, 012008 (2015) Erratum: [Phys. Rev. D **92**, no. 5, 059903 (2015)] [arXiv:1411.1559 [hep-ex]].
- [159] R. Balest *et al.* [CLEO Collaboration], Phys. Rev. D **51**, 2053 (1995).
- [160] P. del Amo Sanchez *et al.* [BaBar Collaboration], Phys. Rev. Lett. **107**, 021804 (2011) [arXiv:1007.4646 [hep-ex]].
- [161] M. Acciarri *et al.* [L3 Collaboration], Phys. Lett. B **345**, 609 (1995).
- [162] E. Anashkin *et al.* [DELPHI Collaboration], CERN-OPEN-99-410, DELPHI-99-137 HEP'99 CONF 324.
- [163] <https://www-cdf.fnal.gov/physics/exotic/r2a/20060908.diphotonPlusX/>
- [164] G. Aad *et al.* [ATLAS Collaboration], Eur. Phys. J. C **76**, no. 4, 210 (2016) [arXiv:1509.05051 [hep-ex]].
- [165] M. Aaboud *et al.* [ATLAS Collaboration], Phys. Lett. B **781**, 55 (2018) [arXiv:1712.07291 [hep-ex]].
- [166] E. Kou *et al.* [Belle II Collaboration], arXiv:1808.10567 [hep-ex].
- [167] H. Baer *et al.*, arXiv:1306.6352 [hep-ph].
- [168] M. Bicer *et al.* [TLEP Design Study Working Group], JHEP **1401**, 164 (2014) [arXiv:1308.6176 [hep-ex]].
- [169] K. Mimasu and V. Sanz, JHEP **1506**, 173 (2015) [arXiv:1409.4792 [hep-ph]].
- [170] J. Jaeckel and M. Spannowsky, Phys. Lett. B **753**, 482 (2016) [arXiv:1509.00476 [hep-ph]].
- [171] S. Knapen, T. Lin, H. K. Lou and T. Melia, Phys. Rev. Lett. **118**, no. 17, 171801 (2017) [arXiv:1607.06083 [hep-ph]].
- [172] A. Mariotti, D. Redigolo, F. Sala and K. Tobioka, Phys. Lett. B **783**, 13 (2018) [arXiv:1710.01743 [hep-ph]].
- [173] A. V. Derbin, I. S. Drachnev, A. S. Kayunov and V. N. Muratova, JETP Lett. **95**, 339 (2012) [Pisma Zh. Eksp. Teor. Fiz. **95**, 379 (2012)] [arXiv:1206.4142 [hep-ex]].
- [174] K. Abe *et al.*, Phys. Lett. B **724**, 46 (2013) [arXiv:1212.6153 [astro-ph.CO]].
- [175] E. Armengaud *et al.*, JCAP **1311**, 067 (2013) [arXiv:1307.1488 [astro-ph.CO]].
- [176] C. E. Aalseth *et al.* [CoGeNT Collaboration], Phys. Rev. Lett. **101**, 251301 (2008) Erratum: [Phys. Rev. Lett. **102**, 109903 (2009)] [arXiv:0807.0879 [astro-ph]].
- [177] Z. Ahmed *et al.* [CDMS Collaboration], Phys. Rev. Lett. **103**, 141802 (2009) [arXiv:0902.4693 [hep-ex]].
- [178] F. Alessandria *et al.* [CUORE Collaboration], JCAP **1305**, 007 (2013) [arXiv:1209.2800 [hep-ex]].
- [179] A. V. Derbin, A. S. Kayunov, V. N. Muratova, D. A. Semenov and E. V. Unzhakov, Phys. Rev. D **83**, 023505 (2011) [arXiv:1101.2290 [hep-ex]].
- [180] G. Bellini *et al.* [Borexino Collaboration], Phys. Rev. D **85**, 092003 (2012) [arXiv:1203.6258 [hep-ex]].
- [181] P. Gondolo and G. G. Raffelt, Phys. Rev. D **79**, 107301 (2009) [arXiv:0807.2926 [astro-ph]].
- [182] G. G. Raffelt, Lect. Notes Phys. **741**, 51 (2008) [hep-ph/0611350].

- [183] R. Essig, R. Harnik, J. Kaplan and N. Toro, Phys. Rev. D **82**, 113008 (2010) [arXiv:1008.0636 [hep-ph]].
- [184] N. Iwamoto, Phys. Rev. Lett. **53**, 1198 (1984).
- [185] D. B. Kaplan, Nucl. Phys. B **260**, 215 (1985).
- [186] A. Sedrakian, Phys. Rev. D **93**, no. 6, 065044 (2016) [arXiv:1512.07828 [astro-ph.HE]].
- [187] R. Mayle, J. R. Wilson, J. R. Ellis, K. A. Olive, D. N. Schramm and G. Steigman, Phys. Lett. B **203**, 188 (1988).
- [188] A. Burrows, M. S. Turner and R. P. Brinkmann, Phys. Rev. D **39**, 1020 (1989).
- [189] G. Raffelt and D. Seckel, Phys. Rev. Lett. **60**, 1793 (1988).
- [190] M. S. Turner, Phys. Rev. Lett. **60**, 1797 (1988).
- [191] M. Giannotti and F. Nesti, Phys. Rev. D **72**, 063005 (2005) [hep-ph/0505090].
- [192] J. H. Chang, R. Essig and S. D. McDermott, JHEP **1809**, 051 (2018) [arXiv:1803.00993 [hep-ph]].
- [193] T. Fischer, S. Chakraborty, M. Giannotti, A. Mirizzi, A. Payez and A. Ringwald, Phys. Rev. D **94**, no. 8, 085012 (2016) [arXiv:1605.08780 [astro-ph.HE]].
- [194] E. G. Adelberger, B. R. Heckel, S. A. Hoedl, C. D. Hoyle, D. J. Kapner and A. Upadhye, Phys. Rev. Lett. **98**, 131104 (2007) [hep-ph/0611223].
- [195] G. L. Klimchitskaya and V. M. Mostepanenko, Eur. Phys. J. C **75**, no. 4, 164 (2015) [arXiv:1503.04982 [hep-ph]].
- [196] G. L. Klimchitskaya, Eur. Phys. J. C **77**, no. 5, 315 (2017) [arXiv:1704.02920 [hep-ph]].
- [197] G. Vasilakis, J. M. Brown, T. W. Kornack and M. V. Romalis, Phys. Rev. Lett. **103**, 261801 (2009) [arXiv:0809.4700 [physics.atom-ph]].
- [198] D. Curtin, P. Meade and C. T. Yu, JHEP **1411**, 127 (2014) [arXiv:1409.0005 [hep-ph]].
- [199] CMS Collaboration [CMS Collaboration], CMS-PAS-HIG-17-008.
- [200] CMS Collaboration [CMS Collaboration], CMS-PAS-HIG-17-002.
- [201] M. Aaboud *et al.* [ATLAS Collaboration], JHEP **1901**, 030 (2019) [arXiv:1804.06174 [hep-ex]].
- [202] <https://fcc.web.cern.ch/Pages/default.aspx>
- [203] J. Baglio, A. Djouadi, R. Gröber, M. M. Mühlleitner, J. Quevillon and M. Spira, JHEP **1304**, 151 (2013) [arXiv:1212.5581 [hep-ph]].
- [204] ATLAS Collaboration, ATL-PHYS-PUB-2013-001.
- [205] F. Goertz, A. Papaefstathiou, L. L. Yang and J. Zurita, JHEP **1306**, 016 (2013) [arXiv:1301.3492 [hep-ph]].
- [206] W. Yao, arXiv:1308.6302 [hep-ph].
- [207] V. Barger, L. L. Everett, C. B. Jackson and G. Shaughnessy, Phys. Lett. B **728**, 433 (2014) [arXiv:1311.2931 [hep-ph]].
- [208] A. J. Barr, M. J. Dolan, C. Englert, D. E. Ferreira de Lima and M. Spannowsky, JHEP **1502**, 016 (2015) [arXiv:1412.7154 [hep-ph]].
- [209] D. M. Asner *et al.*, arXiv:1310.0763 [hep-ph].

- [210] J. Tian *et al.* [ILD Collaboration], PoS EPS -**HEP2013**, 316 (2013) [arXiv:1311.6528 [hep-ph]].
- [211] E. Thrane and J. D. Romano, Phys. Rev. D **88**, no. 12, 124032 (2013) [arXiv:1310.5300 [astro-ph.IM]].